Mitochondrial Alkbh1 localises to mtRNA granules and its knockdown induces mitochondrial UPR in humans and *C. elegans*

Anita Wagner[1#], Olga Hofmeister[1], Stephane G Rolland[2], Andreas Maiser[2], Koit Aasumets[3], Sabine Schmitt[4], Kenji Schorpp[5], Annette Feuchtinger[6], Kamyar Hadian[5], Sabine Schneider[7], Hans Zischka[1,4], Heinrich Leonhardt[2], Barbara Conradt[2], Joachim M Gerhold[3], Alexander Wolf[1*]

[1] Institute of Molecular Toxicology and Pharmacology, Helmholtz Zentrum München-German Research Center for Environmental Health, Ingolstädter Landstrasse 1, 85764 Neuherberg, Germany.

[2] Department of Biology II, Center for Integrated Protein Science Munich, Ludwig-Maximilians-University Munich, 82152 Planegg-Martinsried, Germany.

[3] Institute of Technology, University of Tartu, Nooruse 1, 50411 Tartu, Estonia.

[4] Institute of Toxicology and Environmental Hygiene, School of Medicine, Technical University Munich, 80802 Munich, Germany

[5] Assay Development and Screening Platform, Institute of Molecular Toxicology and Pharmacology, Helmholtz Zentrum München-German Research Center for Environmental Health, Ingolstädter Landstrasse 1, 85764 Neuherberg, Germany.

[6] Institute of Pathology, Helmholtz Zentrum München-German Research Center for Environmental Health, Ingolstädter Landstrasse 1, 85764 Neuherberg, Germany.

[7] Center for Integrated Protein Science at the Department of Chemistry, Chair of Biochemistry, Technical University of Munich, Lichtenbergstrasse 4, 85748 Garching, Germany.

[*] To whom correspondence should be addressed. Tel. 0049-(0)89-31873165; Email: alexander.wolf@helmholtz-muenchen.de

[#] present address: Research Program for Clinical and Molecular Metabolism, Faculty of Medicine, University of Helsinki, Finland

JCS Advance Online Article. Posted on 21 August 2019

ABSTRACT

The Fe(II) and 2-oxoglutarate dependent oxygenase Alkb homolog 1 (Alkbh1) has been shown to act on a wide range of substrates, like DNA, tRNA or histones. Thereby different enzymatic activities have been identified including, amongst others demethylation of N^3-methylcytosine (m^3C) in RNA- and single-stranded DNA-oligonucleotides, demethylation of N^1-methyladenosine (m^1A) in tRNA or formation of 5-formyl cytosine (f^5C) in tRNA. In accordance with the different substrates Alkbh1 has also been proposed to reside in distinct cellular compartments in human and mouse cells, including the nucleus, cytoplasm and mitochondria. Here we describe further evidence for a role of human Alkbh1 in regulation of mitochondrial protein biogenesis, including localisation of Alkbh1 into mitochondrial RNA granules with super-resolution 3D SIM microscopy. Electron microscopy and high-resolution respirometry analyses revealed an impact of Alkbh1 level on mitochondrial respiration, but not on mitochondrial structure. Downregulation of Alkbh1 impacts cell growth in Hela cells and delays development in *C. elegans*, where the mitochondrial role of Alkbh1 seems to be conserved. Alkbh1 knockdown, but not Alkbh7 knockdown, triggers mitochondrial unfolded protein response (UPR^{mt}) in *C. elegans*.

KEY WORDS

RNA modifications, mitochondrial unfolded-protein response, Fe(II) and 2-oxoglutarate dependent oxygenases, Jumonji-domain containing enzymes, RNA granules, mitochondrial structure

INTRODUCTION

The Alkb-homologs (Alkbhs) are a subgroup of the large enzyme superfamily of Fe(II) and 2-oxoglutarate dependent oxygenases (2OG oxygenases) (Fedeles et al., 2015). Enzymes of the 2OG oxygenase family can either catalyse hydroxylation or oxidative demethylation reactions in humans. Thereby the enzymes seem to have a substrate specificity towards either amino acids in proteins or nucleotides in DNA or RNA (Aik et al., 2012). Due to the wide set of potential substrates individual 2OG oxygenases have been reported to be involved in cellular processes, like transcription (Schofield and Ratcliffe, 2004), splicing (Bottger et al., 2015), translation (Zhuang et al., 2015) or epigenetic regulation (Kooistra and Helin, 2012; Yin and Xu, 2016). The 2OG oxygenase-subfamily of Alkbhs comprise nine members in humans, including Alkbh1-8 and Fto (Fedeles et al., 2015). Some Alkbhs are without any identified catalytic activity yet (Alkbh6, Alkbh7). Others demethylate DNA upon alkylation damage (Alkbh2), or modify tRNA molecules at the wobble position (Alkbh8) (Fedeles et al., 2015; Fu et al., 2010a; Fu et al., 2010b; Songe-Moller et al., 2010; van den Born et al., 2011). Fto and Alkbh5 seem to be the major RNA demethylases for N^6-methyladenosine (m^6A) in mRNA (Meyer and Jaffrey, 2014). However, a controversial discussion arose about Alkbh1. By now six distinct enzymatic activities have been reported for the Alkbh1 protein. Initially recombinant human Alkbh1 purified from bacteria has been shown to demethylate N^3-methylcytosine (m^3C) in RNA- and single-stranded DNA-oligonucleotides (ssDNA) (Westbye et al., 2008). In the meantime Alkbh1 has also been implicated in the modification of tRNA. Here Liu et al. have demonstrated a demethylase activity of Alkbh1 towards the m^1A at position 58 in cytoplasmic tRNA (Liu et al., 2016). Alkbh1 knockout cells have an increase in m^1A level in mitochondrial tRNAs too (Kawarada et al., 2017). The Alkbh1-catalysed formation of 5-formyl cytosine (f^5C) from 5-methyl cytosine (m^5C) has been shown for position 34 in cytosolic $tRNA^{Leu}$ (Kawarada et al., 2017) and for position 34 in mitochondrial $tRNA^{Met}$ (Haag et al., 2016). A role in epigenetic regulation has been proposed for the mouse Alkbh1 homolog. Wu et al. described m^6A demethylation of DNA in mouse embryonic stem cells (Wu et al., 2016) and even histone demethylation of histone H2A seems to be catalyzed by Alkbh1 in mouse stem cells (Ougland et al., 2012). Despite the obvious 2OG oxygenase activity Hausinger and colleagues identified a nonoxidative role for Alkbh1 in DNA cleavage at abasic sites (Muller et al., 2010).

All the described individual substrates imply localization of the Alkbh1 enzyme in various distinct cellular compartments, including the nucleus, the cytosol and the mitochondria. Immunofluorescent staining with an anti-Alkbh1 antibody in stem cells suggested a nuclear localization (Ougland et al., 2016; Ougland et al., 2012), whereas anti-Alkbh1 staining in Hela or 293 cells revealed a mitochondrial localization (Haag et al., 2016; Westbye et al., 2008). This mitochondrial localization was supported by the overexpression of a yellow-fluorescent protein (YFP)-tagged human Alkbh1 (Westbye et al., 2008). An *N*-terminal YFP-tag abolished localization to mitochondria and implied a mitochondrial targeting sequence at the *N*-terminus of Alkbh1, although not predictable within the amino acid sequence (Westbye et al., 2008).

In the present study, we describe more detailed investigations on the mitochondrial role of Alkbh1. We analyzed distribution in various different human cell lines and determined Alkbh1 localization to RNA granules in mitochondria by 3D structured illumination microscopy (3D SIM) (Schermelleh et al., 2008) and by flotation gradients (Gerhold et al., 2015). Electron microscopy analysis and high resolution respirometry has been used to investigate the impact of Alkbh1 level on mitochondrial structure and function. Knockdown of Alkbh1 in human cells revealed an increase in expression of the mitochondrial matrix protease Clpp, which seems to play a role in the mitochondrial unfolded protein response (UPR^{mt}) (Haynes et al., 2007; Shpilka and Haynes, 2018; Zhao et al., 2002). In accordance with Clpp upregulation in human cells we also found an initiation of UPR^{mt}, but not endoplasmic reticulum unfolded protein response (UPR^{ER}) in *Caenorhabditis elegans* (*C. elegans*). Knockdown of Alkbh1 results in a proliferation defect in Hela cells and in a delay in development in *C. elegans*. Overall our results support the proposal that human Alkbh1 has a major function in mitochondrial protein biogenesis and that this role is conserved in *C. elegans*.

MATERIALS AND METHODS

Antibodies

The following antibodies were used for Western blot and immunofluorescence staining: anti-Alkbh1 (ab49738, *Abcam*), anti-Alkbh1 (ab126596, *Abcam*), anti-Flag antibody M2 (F1804-200ul, *Sigma*), anti-DNA (AC-30-10, *Progen*), anti-Fastkd2 (17464-1-AP, *Proteintech*), anti-GFP (11814460001, *Roche*), anti-Hsp60 (ab46798, *Abcam*), anti-Tfam (ab119684, *Abcam*), anti-Gapdh (2118 S, *Cell Signaling*), anti-Hsp60 (sc-1052, *Santa Cruz*), anti-mitochondrial Hsp70 (sc-13967, *Santa Cruz*), anti-Clpp (ab124822, *Abcam*), anti-Tfam (Gerhold et al., 2015) (gift from Rudolf Wiesner, University of Cologne, Germany), anti-Twinkle (Gerhold et al., 2015) (gift from Anu Suomalainen Wartiovaara, University of Helsinki, Finland), anti-Mrs35 (ab182160, *Abcam*), anti-Mrpl48 (ab194826, *Abcam*), anti-Ssbp1 (HPA002866, *Sigma*), anti-Tufm (ab175199, *Abcam*). Alexa488 anti-rat, Alexa594 anti-rat, Alexa594 anti-rabbit, Alexa488 anti-mouse (*Life Technologies*) were used as secondary antibodies for immunofluorescence staining.

Cell culture and immunostaining

Hela cells (ATCC CCL-2.2), HT-29 cells (ATCC HTB-38), A549 cells (ATCC CCL-185) and human embryonic kidney (HEK) 293T (ATCC CRL-11268) or 293 cells (ATCC CRL-1573) were cultured in Dulbecco's modified Eagle's medium, human prostate cancer (PC-3) cells (ATCC CRL-1435) were cultured in RPMI medium at 37°C and 5% CO_2. All media were supplemented with 10% fetal calf serum and penicillin/streptomycin (100 U/ml). For microscopy, $3x10^4$ cells were seeded on 18mm glass coverslips and transfected with expression constructs using Lipofectamine 2000 (*Invitrogen*) following the manufacturer's protocol. 24h post-transfection cells were fixed with 4% paraformaldehyd (PFA) for 5min at room temperature (RT) and with ice-cold methanol for 5min on ice. Cells were permeabilised with 1% Triton-X-100 in PBS, blocked in 3% BSA (*Sigma*) and stained with the indicated antibodies and DAPI (1μg/ml). After immunostaining, samples were mounted in Vectashield (*Vector Laboratories*) and stored at 4°C in the dark until analysis with either a fluorescence microscope Carl Zeiss LSM 510 META or a 3D SIM Deltavision OMX V3 microscope (*General Electric*).

Super-resolution microscopy (3D-SIM)

Super resolution imaging was performed with a 3D SIM Deltavision OMX V3 microscope (*General Electric*) equipped with a 100 × 1.4 oil immersion objective UPlanSApo (*Olympus*), 405 nm, 488 nm and 593 nm diode lasers and Cascade II EMCCD cameras (*Photometrics*). With the softWoRx 6.0 Beta 19 (unreleased) software, 3D SIM raw data were first reconstructed and corrected for color shifts. In a second step, a custom-made macro in Fiji (Schindelin et al., 2012) was used to finalize the channel alignment and to establish composite TIFF stacks that are subsequently loaded as leveled RGB images into the Volocity calculation software (Volocity 6.1.2 (*Perkin Elmer*)). Here, structures were obtained, segmented and measured in all channels by using the threshold commands "Find Objects", "Separate Touching Objects" and "Exclude Objects by Size". Co-localizing structures were segmented and measured with the "Intersect" command and quantified according to volume and number.

Knockdown of human Alkbh1 with siRNAs

293 cells were transfected with siRNAs (*Life Technologies*) targeting human Alkbh1 using 50nM siRNA and Lipofectamine 2000 (*Invitrogen*) in Opti-MEM according to manufacturer´s instructions. Cells were harvested 24h after transfection and analyzed by Western Blotting using the indicated antibodies. The Alkbh1 siRNA sequences were GGUAUAAAGAAGCGACUAATT (AM17144, *Life Technologies*) and GGCACCUGCUUACCGUAAATT (AM107924, *Life Technologies*). As negative control we used the Silencer™ Negative control No.1 siRNA (AM4611, *Life Technologies*).

Mitochondrial respiration

Mitochondrial respiration was measured in an Oxygraph-2k instrument (Oroboros Instruments, Innsbruck, Austria). In more detail, 2 million cells were added to the chamber containing 2ml buffer (8mM KCl, 110mM potassium-gluconate, 10mM NaCl, 10mM Hepes, 10mM K_2HPO_4, 15µM EGTA (K^+ salt), 0.5 mg/ml BSA (FA free), 10mM Mannitol, pH adjusted to 7.25) with 5mM NaF, 200µM $BeSO_4$, 25mM $NaVO_3$, 50µM Ap5A, 1mM $MgCl_2$ and 1.1µM Magnesium Green. Cells were permeabilised with 1µg/million cells (control siRNA, Alkbh1 siRNA1) or 0.5µg/million cells (Alkbh1 siRNA2), respectively. Glutamate (final 10mM), Malate (final 2mM) and Succinate (final 25mM) were used as substrates and ADP (final 2.5mM) was added to measure oxidative Phosphorylation. The capacity of the electron transport system was determined upon addition of Carbonyl Cyanide m-Chlorophenylhydrazone CCCP (final 5µM) and non-mitochondrial respiration was determined upon addition of Antimycin A (final 500nM).

Generation of inducible, stable cell lines

We used a technique described by Wiznerowic and Trono (Wiznerowicz and Trono, 2003) to establish doxycycline inducible Hela cell lines. Overexpressing cell lines either express untagged Alkbh1 or a GFP sequence targeted to mitochondria (mitoGFP, *Clontech*). For RNA interference we cloned small hairpin RNA into the lentiviral vector pLVTHM. This plasmid was co-transfected with the packaging plasmid psPAX2 and the envelope plasmid pMD2.G. The viral particles were collected and used to transduce Hela cells containing the pLV-tRKRAB plasmid. Alkbh1-specific shRNA sequences were GACCGTAGGCTACCATTATAA (sh-5017), TGACCAGAATAGCGAAGTAAA (sh-5020) and GAGGTATAAAGAAGCGACTAA (sh-7996). An unspecific control shRNA (AATTCTCCGAACGTGTCACGT) was used as described before (Bognar et al., 2016).

Quantification of cell number

Inducible stable cell lines were seeded in poly-d-lysine hydrobromide (50 μg/ml, *Sigma*) coated 96-well plates and induced with Doxycyclin (250ng/ml, *Sigma*) each day (24h intervals). Cell numbers were determined every 24h for 6 days. Cells were fixed with 4% PFA and stained with 1μg/ml DAPI in PBST for 5 minutes. Cells were imaged on an automated *Operetta* High-Content microscope (*Perkin Elmer*) with a 10x LW objective for high-resolution images. 15 images per well were recorded. Quantification of cell number per well was performed using Columbus Software 2.8.0 (*Perkin Elmer*). Here nuclei were detected via the DAPI signal. In a next step morphology of all identified objects were calculated and only objects with a specific size (<1000μm^2) and roundness (>0.75) were selected for analysis. The number of those nuclei per well was determined.

Isolation of mitochondria

For isolation of intact mitochondria cells were homogenized and ruptured in isolation buffer (300 mM sucrose, 5 mM *N*-tris(hydroxymethyl) methyl-2-aminoethanesulfonic acid (TES) and 200 μM ethleneglycoltetraacetic acid (EGTA, pH 7.2)) using the pump-controlled cell rupture system (PCC) described in (Schmitt et al., 2013). 293T cells were passed through the system in a suspension of $7*10^6$ cells/ml for six times and a clearance of 8 μm. For isolation from A549 cells, a cell density of $7*10^6$ cells/ml and three strokes with a clearance of 8 μm were used. Isolation of Hela cell mitochondria were performed with a cell density of $4*10^6$ cells/ml, 6 μm clearance and three strokes. Cells were passed through the system with a constant speed rate of 700 μl/min.

A centrifugation step (800g, 5 min at 4°C) was carried out to clear the homogenate from cell debris and nuclei. Another centrifugation step was performed at 9000g (10 min at 4°C) to pellet intact mitochondria. Isolation of mitochondria was validated in immunoblots for mitochondrial marker proteins.

Flotation gradients of mitochondrial fractions

Mitochondria from 293 cells were pepared as previously described (Gerhold et al., 2015; Rajala et al., 2014). In brief, cells were collected and resuspended in hypotonic buffer (4 mM Tris-HCl, pH 7.8, 2.5 mM NaCl, 0.5 mM $MgCl_2$ and 2 mM PMSF), allowed to swell for 6 min and disrupted with 20-25 strokes with a tight-fitting Potter-Elvehjem homogenizer on ice. The suspension was isotonised with 400 mM Tris-HCl, 250 mM NaCl and 50 mM $MgCl_2$ and centrifuged at 1200 g for 5 min at 4 °C (removal of nuclei and cell debris). This step was repeated once and crude mitochondria were subsequently pelleted from the cytosolic supernatant by centrifugation at 13000 g for 10 min at 4 °C.

Flotation gradients of mitochondrial fractions were carried out as described (Gerhold et al., 2015; Rajala et al., 2014). Mitochondrial membranes of purified mitochondria (the equivalent to 1 mg of total mitochondrial protein) were disrupted using digitonin (*Sigm-Aldrich*) at a ratio (μg digitonin/μg protein) of 2/1 in PBS including protease inhibitors (*Applichem*). Reactions were incubated on ice for 10 min followed by centrifugation at 14000 g for 10 min at 4°C to obtain a membrane enriched pellet (yielding membrane-associated components) and a supernatant containing soluble components. The pellet-fraction was resuspended in TN buffer (25 mM Tris-HCl, pH 7.8, 150 mM NaCl, 1 mM DTT, protease inhibitors, 10% sucrose, 1% Triton X-100) at 4°C. Both, the pellet and the supernatant fractions were mixed with cold OptiprepTM to a final concentration of 42.5%, transferred to MLS-55 centrifuge tubes and overlaid with an 8-step OptiprepTM gradient (40, 37.5, 35, 32.5, 30, 27.5, 25, 20, 0%) prepared in TN. The gradients were centrifuged at 100000 g for 14h at 4°C. Fractions (400 μl) were collected from the top and analysed for proteins by western blots and for mtDNA by dot blots. Here, 20 μl of sample was diluted in 380 μl of 2x SSC, boiled for 15 min at 95°C and blotted onto positively charged nylon membranes (Hybond, *GE Healthcare*). The dot blots were hybridized at 68°C with ^{32}P-dCTP-labelled probes against Cytb (for: TGAAACTTCGGCTCACTCCT, rev: GTTGTTTGATCCCGTTTCGT) and detected with a Typhoon-phosphoimager (*GE Healthcare*).

Alkbh1 and Alkbh7 in *C.elegans*

The cDNA of *Y51H7C.5* (homolog of Alkbh1 in *C. elegans*) and *Y46G5A.35* (homolog of Alkbh7 in *C. elegans*) were amplified by PCR and cloned blunt into the EcoRV site of the pBlueScript II SK vector (*Stratagene*) to generate the plasmids pBC1595 and pBC1596, respectively. The cDNA fragments were re-amplified from these plasmids using the primers CMO24 (5'-ttgtaaaacgacggccag-3') and CMO25 (5'- catgattacgccaagcgc-3') and used as template to generate ssRNA using the T7 and T3 Megascript in vitro transcription kits (*Invitrogen*). A negative control was performed using the plasmid pBC1152, which contains the *tag-208* cDNA cloned into the pBlueScript II SK vector. To generate dsRNA, equal moles of ssRNA were annealed by incubating them at 75°C for 5 minutes and at 20°C for 10 minutes. 10 adults of N2 (24 hours post L4 larval stage) were injected with *tag-208*, *Y51H7C.5* or *Y46G5A.35* dsRNA. After 24 hours of incubation at 20°C, the injected animals were transferred singly onto a new plate and let to lay eggs for 4 hours. The injected animals were then removed and the plates were further incubated at 20°C. 72 hours post lay-off, the developmental stage of the progeny of the injected animals was analyzed. The number of gravid adults, young adults and L4 larvae was quantified. Three independent experiments were performed with 2-3 plates analyzed in each experiment.

To analyze the effect of *Y51H7C.5* and *Y46G5A.35* knockdown on mitochondrial unfolded protein response (UPR^{mt}) and endoplasmic reticulum unfolded protein response (UPR^{ER}), experiments were performed essentially as described above with the exception that dsRNA was injected into SJ4100 animals (which carry the mitochondrial chaperone *hsp-6* transcriptional reporter), into SJ4058 animals (which carry the mitochondrial chaperone *hsp-60* transcriptional reporter) and into SJ4005 animals (which carry the ER chaperone *hsp-4* transcriptional reporter). Brightfield and fluorescent images of the progeny were taken 96 hours post lay-off using a Leica GFP dissecting microscope (M205FA) and the software Leica Application Suite (3.2.0.9652).

Mitochondrial extraction from *C. elegans*

We generated *Y51H7C.5::GFP* and *Y51H7C.5::HA* fusion construct by fusion PCR and subcloned these constructs into the heat-inducible vectors (pPD49.78 and pPD49.83) to generate the plasmids (pPD49.78:Y51H7C.5::GFP, pPD49.83:Y51H7C.5::GFP, pPD49.78:Y51H7C.5::HA, and pPD49.83:Y51H7C.5::HA, respectively). pPD49.78:Y51H7C.5::GFP and pPD49.83:Y51H7C.5::GFP were co-injected at 5 ng/µl (each) with pRF4 (80 ng/µl) in N2 animals to generate the transgenic line MD4000. pPD49.78:Y51H7C.5::HA and pPD49.83:Y51H7C.5::HA were co-injected at 5 ng/µl (each) with pRF4 (80 ng/µl) in N2 animals to generate the transgenic line MD4199. For mitochondrial extraction, MD4199 animals were cultured on eight large NGM plates at 20 °C and then heat-shocked at 30°C for 1h 15 min to allow the expression of the transgene. After 1 h 30 min of recovery at 20°C, mitochondria were extracted as described previously (Lu et al., 2011). Total lysate, post mitochondrial supernatant, and mitochondria-enriched fraction were analyzed by SDS-PAGE. To detect HSP60, Tubulin and Y51H7C.5::HA, we used anti-HSP60 (Hadwiger et al., 2010), anti-αTubulin (*Sigma*) and anti-HA (*Sigma*) antibodies, respectively. HSP60 was deposited to the DSHB by Nonet, M.L., Hadwiger, G. and Dour, S. (DSHB Hybridoma Product HSP60).

RESULTS

Alkbh1 localizes to mitochondrial RNA (mtRNA) granules

As there have been controversial reports about intracellular localisation of human Alkbh1 we initially analysed its distribution using immunofluorescence and mitochondria isolation (Schmitt et al., 2013) approaches in various different human cell lines, including Hela (cervix carcinoma cells), 293T (embryonic kidney cells), A549 (lung carcinoma cells), PC3 (prostate cancer cells) and HT-29 (colorectal adenocarcinoma cells). Ectopic expression of the untagged human Alkbh1 full-length sequence (Uniprot: Q13686) resulted in a mitochondrial localisation in the analysed cell lines, as confirmed by co-localisation with a mitochondrial GFP (mitoGFP) (**Fig. 1A-C**). Staining of endogenous Alkbh1 co-stained with a transient mitoGFP signal confirmed the mitochondrial localisation (**Fig. S1A-C**). Furthermore anti-Alkbh1 immunoblots gave a prominent Alkbh1 signal in

mitochondrial fractions after isolation of mitochondria from Hela, 293T and A549 cells. The pattern resembled the distribution of the mitochondrial marker protein HSP60 (**Fig. 1D**).

We used super-resolution microscopy and 3D-SIM (3D structured illumination microscopy) reconstruction (Schermelleh et al., 2008) of A549 cells to investigate the submitochondrial localization of Alkbh1. Alkbh1 has been shown to localize to the mitochondrial matrix (Westbye et al., 2008). We stained cells with an anti-Alkbh1 antibody and co-stained for the mitochondrial nucleoid with an anti-DNA antibody as described previously (Kukat et al., 2011) (**Fig. 2A**) or for the mitochondrial RNA (mtRNA) granules with an anti-Fastkd2 antibody (Antonicka and Shoubridge, 2015) (**Fig. 2B**). Both, nucleoids and mtRNA granules are nucleoprotein assemblies in close regional vicinity in the mitochondrial matrix (Pearce et al., 2017). Overlap analysis revealed Alkbh1 colocalisation with the mtRNA granule marker protein Fastkd2 and less overlap with the anti-mtDNA staining (**Fig. 2C**).

Majority of Alkbh1 co-fractionates with mtRNA granule components and the mitochondrial ribosomal proteins

In a next step Alkbh1 distribution in mitochondria was analyzed by specific bottom-up density gradient centrifugation i.e. flotation gradients. This method has been applied recently to investigate mitochondrial DNA-protein complexes (Gerhold et al., 2015; Rajala et al., 2014). We purified mitochondria from 293 cells and after treatment with digitonin, mitochondria were centrifuged (see `Materials and Methods´ section). This procedure results in an insoluble mitochondrial membrane pellet fraction including also protein complexes tightly associated with the inner mitochondrial membrane (IMM) while soluble components are found in the supernatant (Gerhold et al., 2015; Rajala et al., 2014). Both, pellet and supernatant, were subjected to bottom-up centrifugation through stepwise lowering concentrations of iodixanol (OptiPrep) (**Fig. 3A**). Earlier experiments showed that in such a fractionation approach the mtDNA and associated proteins, like Twinkle accumulate mainly in the low-density fraction 8, as exemplified in western blots stained for marker proteins (Gerhold et al., 2015; Rajala et al., 2014). Our experiments confirmed this discrete concentration of mtDNA into fraction 8 (**Fig. 3B**). In contrast, anti-Alkbh1 staining revealed no obvious co-fractionation of Alkbh1 with the nucleoid fraction (**Fig. 3C**). Most of the anti-Alkbh1 signal was found in fractions 1-4, but some weak signal seemed to appear in fraction 8 too (**Fig 3C**). In accordance with our high-resolution imaging approaches the Alkbh1 fractionation pattern resembled the distribution of the mtRNA granule marker protein Fastkd2 and the mitochondrial translation elongation factor Tufm. Both accumulated mainly in fractions 1-5 and showed weak signal in fraction 8 (**Fig. 3D**). Proteins linked to mitochondrial translation, like the mitochondrial ribosomal protein Mrpl48 of the large 39S subunit (mtLSU) and Mrps35 of the small 28S subunit were also mainly detectable in fraction 2-5 and showed no overlap with the mtDNA fraction 8 (**Fig. 3D**).

In summary our different approaches to analyse submitochondrial localization of Alkbh1 point consistenly towards a link to mtRNA granules and mitochondrial translation, supporting the proposal of Alkbh1-catalysed tRNA modifications in mitochondria and subsequent impact on mitochondrial translation (Haag et al., 2016).

Knockdown of Alkbh1 upregulates the mitochondrial unfolded protein response (UPR^{mt}) in human cells

Dysregulation of mitochondrial translation and a subsequent accumulation of damaged or unfolded proteins in the mitochondrial matrix can activate the mitochondrial unfolded protein response (UPR^{mt}) in order to maintain mitochondrial function (Shpilka and Haynes, 2018). This adaptive mitochondrial stress response results in an increased transcription of mitochondrial chaperones and proteases, like the mitochondrial matrix protease Clpp. Clpp cleaves misfolded proteins into peptides and is thought to play a role in UPR^{mt} initiation in *C. elegans* (Shpilka and Haynes, 2018; Zhao et al., 2002). We analysed the upregulation of human Clpp upon Alkbh1 knockdown in 293 cells. An siRNA-mediated knockdown with two specific Alkbh1-siRNAs resulted in an increase of Clpp protein level after 24 hours if compared to cells treated with an unspecific siRNA (**Fig. 4+S4**).

To confirm our UPR^{mt} findings from human cells we used *C. elegans*, which is an established model for genetic and biochemical studies of UPR^{mt}, in which several key components of the pathway regulating UPR^{mt} have been identified (Haynes et al., 2007; Haynes et al., 2010; Nargund et al., 2012) .

Y51H7C.5, the homolog of Alkbh1 in *C. elegans*, partially localizes to mitochondria

Analysis of the *C. elegans* genome identified Y51H7C.5 as a putative homolog of human Alkbh1 (Greer et al., 2015; Kollarova et al., 2018). Y51H7C.5 shares 28,1% identity and 37,5% similarity with the human Alkbh1 protein (**Fig. S2**). We first decided to determine whether, like human Alkbh1, the *C. elegans* Alkbh1 (ceAlkbh1) protein localizes to mitochondria. Analysis of the protein sequence using the software MitoProt (https://ihg.gsf.de/ihg/mitoprot.html) revealed that ceAlkbh1 is likely to be targeted to mitochondria (probability 0.4085) and that its mitochondrial targeting sequence is predicted to be 36 amino acids (aa) long (aa1-36). In order to confirm the localization of ceAlkbh1, we initially generated a *C*-terminal GFP fusion that was placed under the control of a heat-inducible promoter. After heat-shock, the ceAlkbh1::GFP fusion protein seems to localize to the cytosol (data not shown). However, since GFP could have prevented the proper localization of the fusion protein, as described for human Alkbh1 (Westbye et al., 2008), we therefore decided to use a smaller tag and generated a *ceAlkbh1::HA* fusion construct also expressed under the control of a heat-inducible promoter. We first confirmed that upon heat-shock the construct is expressed and has the correct molecular weight using anti-HA antibodies (42 kDa) (**Fig. 5A**). We, then, performed a cell fractionation experiment. As shown in **Fig. 5B**, tubulin is only found in the post mitochondrial fraction (PMS), which corresponds to the cytosolic fraction. In contrast, the mitochondrial chaperone Hsp60, which is a mitochondrial matrix protein, is mostly found in the mitochondrial-enriched fraction (M). The ceAlkbh1::HA is found in both fractions. Altogether these data indicate that Alkbh1 localizes at least partially to mitochondria in *C. elegans*.

Inactivation of ceAlkbh1 triggers UPR^{mt} in *C. elegans*

To analyze the effect of knockdown of ceAlkbh1 on UPR^{mt} we used two *C. elegans* UPR^{mt} reporter strains (Yoneda et al., 2004). In more detail we used the strain SJ4100, in which the GFP sequence is under the control of the promoter of the mitochondrial chaperone *hsp-6* (which is the homolog of the human mitochondrial Hsp70) and the strain SJ4058, in which the GFP sequence is under the control of the promoter of the mitochondrial chaperone *hsp-60* (which is the homolog of the human mitochondrial Hsp60). As a negative control we used a strain, which carries the endoplasmic reticulum (ER) chaperone *hsp-4* transcriptional reporter (SJ4005), an indicator for endoplasmic reticulum UPR (UPR^{ER}). Induction of either UPR^{mt} or UPR^{ER} was monitored by following the level of GFP expression in the reporter strains. In order to knockdown ceAlkbh1 level in *C. elegans*, we injected ceAlkbh1 dsRNA and as a negative control we used dsRNA targeting an unrelated gene *tag-208*. As an additional control, we used dsRNA targeting *Y46G5A.35*, which encodes the potential *C. elegans* homolog of human Alkbh7 (ceAlkbh7) (Uniprot: Q7YWP5; Ensembl gene: WBGene00012920). The human Alkbh7 is another 2OG oxygenase of the Alkb-homologs subfamily which has been reported to also localize to mitochondria in Hela cells (Fu et al., 2013). *C. elegans* Y46G5A.35 (ceAlkbh7) shares 36.1% identity at the amino acids level with human Alkbh7 (Uniprot: Q9BT30; Ensembl gene: ENSG00000125652) (**Fig. S3**). As shown in Figure 5, knockdown of the ceAlkbh1 induces the transcriptional activation of the *Phsp-6GFP* and *Phsp-60GFP* reporters but not of the *Phsp-4GFP* reporter (**Fig. 5C-E**). In contrast, none of the reporter is up-regulated in response to the inactivation of the ceAlkbh7 (**Fig. 5C-E**). Altogether these results indicate that, similar to what was observed in mammalian cells, the loss of ceAlkbh1 function leads to the induction of UPR^{mt} in *C. elegans*.

Inactivation of ceAlkbh1 slows down *C. elegans* development

While testing the effect of the inactivation of ceAlkbh1 on UPR^{mt}, we observed that knockdown of ceAlkbh1 affects *C. elegans* development. In order to analyze the effect in more detail, N2 adults (24 hours post L4 larval stage) were injected with either of the three dsRNA (ceAlkbh1, ceAlkbh7 or *tag-208*) and the injected animals were transferred singly onto a new plate and let to lay eggs for 4 hours. Comparing the developmental stage of the progeny 72 hours post lay-off showed gravid adults for almost all *tag-208* dsRNA injected animals, whereas the progeny of ceAlkbh1-dsRNA injected animals consisted of L4 larvae and young adults with no gravid adults. In contrast, the progeny of ceAlkbh7-dsRNA injected animals reached the same developmental stage as the *tag-208*-dsRNA injected animals with all progeny being gravid adults (**Fig. 6A**). To investigate whether knockdown of Alkbh1 results in a complete block of worm development we extended the analysis of developmental stages of knockdown animals to 96 hours post lay-off. Here the development of Alkbh1 knockdown animals seemed to catch up with control animals (**Fig. 6B**).

An impact of Alkbh1 protein level on proliferation of human cells has been described previously too (Haag et al., 2016; Liu et al., 2016), but a controversial effect of Alkbh1-knockdown in Hela cells has been reported. Liu et al. detected an increase in proliferation of Hela cells upon Alkbh1 knockdown (Liu et al., 2016), whereas in contrast Haag et al. described a decrease in growth rate of Hela cells (Haag et al., 2016).

Alkbh1 protein levels impact cell numbers and cellular oxygen consumption

To investigate effects of Alkbh1 protein level on cells, we generated doxycycline-inducible Alkbh1 knockdown Hela cell lines. Lentiviral transduction as described previously (Wiznerowicz and Trono, 2003) was used to incorporate either Alkbh1-specific shRNAs (sh-5017; sh-5020; sh-7996) or an unspecific none-silencing shRNA (ns-shRNA). In addition we generated an inducible Alkbh1 overexpressing Hela cell line (Alkbh1-OE) or a cell-line overexpressing a mitochondrial GFP (mitoGFP-OE) (**Fig. 7A**). In our hands induction of the Alkbh1-specific shRNAs and subsequent decrease in Alkbh1 protein level resulted in a significant decline in cell numbers after six days of treatment when compared to the ns-shRNA (**Fig. 7B**). In accordance, an induction of overexpression of untagged Alkbh1 in Hela cells revealed an increase in cell numbers over a similar time period when compared to cells that overexpress a mitochondrial GFP (**Fig. 7C**). These results are in line with previous observations by Haag et al. (Haag et al., 2016).

To further investigate whether alterations in Alkbh1 protein levels impact mitochondrial structure and/or function, we applied electron microscopy (EM) and high-resolution respirometry (HRR) to 293 cells transiently transfected with siRNAs (Alkbh1 siRNA1, Alkbh1 siRNA2, control siRNA). AlkBH1 knockdown cells revealed no obvious differences in mitochondrial structure compared to control cells (**Fig. 7D-F**). In HRR, a similar respiration in the LEAK state, i.e. in the presence of substrates that fuel the electron transport chain but in the absence of ADP, was observed for Alkbh1 knockdown and control cells (**Fig. 7G**), indicating a comparable mitochondrial membrane integrity. However, mitochondrial oxidative phosphorylation (OXPHOS) and electron transport system (ETS) capacity was affected by the Alkbh1 level, as a significantly lower increase in oxygen consumption was determined in Alkbh1 knockdown compared to control cells upon ADP and CCCP addition, respectively (**Fig. 7G**).

DISCUSSION

We have shown that Alkbh1 localises to mitochondria in various different human cell lines and in *C. elegans*. Nuclear encoded mitochondrial proteins are synthesized by cytosolic ribosomes (Neupert, 2015). Translocation into mitochondria is in most cases mediated via an *N*-terminal mitochondrial targeting sequence (MTS) which is proteolytically removed upon import (Mossmann et al., 2012). Available MTS prediction tools did not detect such an MTS in human Alkbh1 (Westbye et al., 2008). However, the analysis of the *C. elegans* Alkbh1 homolog also revealed mitochondrial localisation and in this case an MTS was predicted for aa 1-36 of the full-length sequence (Y51H7C.5). A sequence comparison showed no corresponding residues in the human Alkbh1 sequence for such a worm-specific *N*-terminal extension (**Fig. S2**). However, expression patterns of transiently expressed untagged human full-length Alkbh1 and endogenous Alkbh1 showed mitochondrial localization.

A closer analysis using a super-resolution 3D-SIM imaging approach (Schermelleh et al., 2008) revealed overlap of mitochondrial Alkbh1 with the mitochondrial RNA granule marker protein Fastkd2 (Antonicka and Shoubridge, 2015) in human A549 cells. However, there was also some overlap detectable with mtDNA in such an approach. We were able to show similar results in specific bottom-up density gradient centrifugation. Performance of Alkbh1 in such flotation gradients resembled the pattern of mtRNA granule proteins, like Fastkd2 and Tufm and mitochondrial ribosomal proteins. Alkbh1 does not seem to be a mitochondrial nucleoid associated protein (NAP) (Hensen et al., 2014), although we have seen some overlap with mtDNA in super resolution microscopy and co-migration with a small subset of nucleoids in flotation gradients. The fact that Alkbh1 shows colocalisation with mtRNA granule markers in IF and biochemical fractionations further stresses involvement of Alkbh1 in translation rather than transcription.

Alkbh1 is a member of the Alkb-homologs, a subgroup of the enzyme superfamily of 2OG oxygenases (Fedeles et al., 2015; Islam et al., 2018). Several Alkbhs have been shown to modify nucleotides in DNA or RNA, like Alkbh5 which demethylates m^6A in mRNA (Meyer and Jaffrey, 2014) or Alkbh8 which modifies uridines at the wobble position in cytosolic tRNA molecules (Fu et al., 2010a; Fu et al., 2010b; Songe-Moller et al., 2010). A mitochondrial nucleotide-modifying enzyme, e.g. Alkbh1 would have several potential nucleotide substrates, including the mtDNA which gets transcribed in polycystronic mRNA molecules which are then further processed into mitochondrial tRNAs, rRNAs and mRNAs (Pearce et al., 2017). Our results showing localisation of Alkbh1 into mtRNA granules support the proposal of Alkbh1 activity towards mitochondrial tRNAs which has been identified recently (Haag et al., 2016). In this study, the authors have shown that Alkbh1 oxidises m^5C at position 34 in mitochondrial $tRNA^{Met}$ to generate f^5C (Haag et al., 2016). Mitochondrial RNA granules are thought to act as hubs for posttranscriptional RNA processing (Antonicka and Shoubridge, 2015). They mainly harbor proteins involved in RNA metabolism and ribosomal proteins (Antonicka and Shoubridge, 2015; Pearce et al., 2017).

However, a decline in Alkbh1 protein level at normal conditions has a significant effect on proliferation in human cells. We saw a decrease of cell numbers upon shRNA-mediated knockdown of Alkbh1 in Hela cells as described before (Haag et al., 2016). In accordance overexpression of Alkbh1 in Hela cells resulted in an increase of cell growth. These growth rate effects in Hela cells have been detected in standard media (4,5 g/l glucose) whereas others described growth rate defects in Alkbh1-deficient 293 cells only in galactose media (Muller et al., 2018). These results and previous data (Kawarada et al., 2017) pointed towards mitochondrial dysfunction in Alkbh1-deficient cells. Our analyses supported those findings and detected an impact of Alkbh1 level on mitochondrial respiration, whereas mitochondrial structure seemed to be unaffected by Alkbh1 knockdown.

In *C. elegans* Alkbh1 is present in mitochondria and the sequence is well conserved. Knockdown of the ceAlkbh1 protein delayed development in *C. elegans* and led to an induction of UPR^{mt} in reporter strains, but showed no effect on UPR^{ER}. Disruption of mitochondrial proteostasis can activate UPR^{mt} (Melber and Haynes, 2018). In the case of ceAlkbh1 a scenario of mitochondrial translation defects due to alterations in tRNA modifications seems likely. Human Alkbh1 can modify mitochondrial tRNA and its knockdown has been linked to protein level changes of mtDNA encoded proteins (Haag et al., 2016). In line with this data we also detected an upregulation of the UPR^{mt} marker Clpp in human cells upon Alkbh1 knockdown. In contrast, Alkbh7, another 2OG oxygenase of the Alkbh subfamily supposed to reside in mitochondria (Fu et al., 2013) has no effect on UPR^{mt} or worm development. The catalytic activity or potential mitochondrial substrates of Alkbh7 are not known yet, neither in mammalian cells nor in *C. elegans*.

Another interesting aspect of a mitochondrial 2OG oxygenase is the fact that the 2OG oxygenase enzyme family has emerged as a potential direct target for changes in cellular metabolism, including pathological conditions like cancer metabolism (Reid et al., 2017). All known 2OG oxygenases use the tricarboxylic acid (TCA) cycle intermediate 2-oxoglutarate (2OG) as a co-substrate, which is essential for their enzymatic activity (Islam et al., 2018). Other TCA cycle intermediates like succinate and fumarate or oncometabolites, like 2-hydroxyglutarate have been identified as inhibitors of 2OG oxygenases (Reid et al., 2017). Therefore alterations in intracellular levels of such metabolites have been shown to impact activity of nuclear 2OG oxygenases involved in for instance epigenetic regulation (TET enzymes) (Reid et al., 2017) or DNA repair (Alkbh2, Alkbh3) (Chen et al., 2017; Wang et al., 2015). The TCA cycle occurs in mitochondria and having a mitochondrial 2OG oxygenase, i.e. Alkbh1, which might be able to sense metabolic alterations and link them directly to mitochondrial protein biogenesis is an intriguing idea, which also merits further investigation.

Acknowlegdements

We thank Dr Michelle Vincendeau (Institute of Virology, Helmholtz Zentrum München, Germany) for her technical advice on the lentiviral transduction system. We thank Carola Eberhagen (Institute of Molecular Toxicology & Pharmacology, Helmholtz Zentrum München) for her support with EM imaging. We thank Juste Wesche (Institute of Molecular Toxicology & Pharmacology, Helmholtz Zentrum München) for her support with ImageJ analysis.

Funding

This work was supported by the Estonian Research Council [PUT610 to J.M.G. and K.A.]; the Deutsche Forschungsgemeinschaft (SFB1064/A17 to H.L. and SCHN 1273/3 to S.S.); and the Nanosystems Initiative Munich, NIM (to H.L.).

References

Aik, W., McDonough, M. A., Thalhammer, A., Chowdhury, R. and Schofield, C. J. (2012). Role of the jelly-roll fold in substrate binding by 2-oxoglutarate oxygenases. *Curr Opin Struct Biol* **22**, 691-700.

Antonicka, H. and Shoubridge, E. A. (2015). Mitochondrial RNA Granules Are Centers for Posttranscriptional RNA Processing and Ribosome Biogenesis. *Cell Rep*.

Bognar, M. K., Vincendeau, M., Erdmann, T., Seeholzer, T., Grau, M., Linnemann, J. R., Ruland, J., Scheel, C. H., Lenz, P., Ott, G. et al. (2016). Oncogenic CARMA1 couples NF-kappaB and beta-catenin signaling in diffuse large B-cell lymphomas. *Oncogene* **35**, 4269-81.

Bottger, A., Islam, M. S., Chowdhury, R., Schofield, C. J. and Wolf, A. (2015). The oxygenase Jmjd6--a case study in conflicting assignments. *Biochem J* **468**, 191-202.

Chen, F., Bian, K., Tang, Q., Fedeles, B. I., Singh, V., Humulock, Z. T., Essigmann, J. M. and Li, D. (2017). Oncometabolites d- and l-2-Hydroxyglutarate Inhibit the AlkB Family DNA Repair Enzymes under Physiological Conditions. *Chem Res Toxicol* **30**, 1102-1110.

Fedeles, B. I., Singh, V., Delaney, J. C., Li, D. and Essigmann, J. M. (2015). The AlkB Family of Fe(II)/alpha-Ketoglutarate-dependent Dioxygenases: Repairing Nucleic Acid Alkylation Damage and Beyond. *J Biol Chem* **290**, 20734-42.

Fu, D., Brophy, J. A., Chan, C. T., Atmore, K. A., Begley, U., Paules, R. S., Dedon, P. C., Begley, T. J. and Samson, L. D. (2010a). Human AlkB homolog ABH8 Is a tRNA methyltransferase required for wobble uridine modification and DNA damage survival. *Mol Cell Biol* **30**, 2449-59.

Fu, D., Jordan, J. J. and Samson, L. D. (2013). Human ALKBH7 is required for alkylation and oxidation-induced programmed necrosis. *Genes Dev* **27**, 1089-100.

Fu, Y., Dai, Q., Zhang, W., Ren, J., Pan, T. and He, C. (2010b). The AlkB domain of mammalian ABH8 catalyzes hydroxylation of 5-methoxycarbonylmethyluridine at the wobble position of tRNA. *Angew Chem Int Ed Engl* **49**, 8885-8.

Gerhold, J. M., Cansiz-Arda, S., Lohmus, M., Engberg, O., Reyes, A., van Rennes, H., Sanz, A., Holt, I. J., Cooper, H. M. and Spelbrink, J. N. (2015). Human Mitochondrial DNA-Protein Complexes Attach to a Cholesterol-Rich Membrane Structure. *Sci Rep* **5**, 15292.

Greer, E. L., Blanco, M. A., Gu, L., Sendinc, E., Liu, J., Aristizabal-Corrales, D., Hsu, C. H., Aravind, L., He, C. and Shi, Y. (2015). DNA Methylation on N6-Adenine in C. elegans. *Cell* **161**, 868-78.

Haag, S., Sloan, K. E., Ranjan, N., Warda, A. S., Kretschmer, J., Blessing, C., Hubner, B., Seikowski, J., Dennerlein, S., Rehling, P. et al. (2016). NSUN3 and ABH1 modify the wobble position of mt-tRNAMet to expand codon recognition in mitochondrial translation. *EMBO J* **35**, 2104-2119.

Hadwiger, G., Dour, S., Arur, S., Fox, P. and Nonet, M. L. (2010). A monoclonal antibody toolkit for C. elegans. *PLoS One* **5**, e10161.

Haynes, C. M., Petrova, K., Benedetti, C., Yang, Y. and Ron, D. (2007). ClpP mediates activation of a mitochondrial unfolded protein response in C. elegans. *Dev Cell* **13**, 467-80.

Haynes, C. M., Yang, Y., Blais, S. P., Neubert, T. A. and Ron, D. (2010). The matrix peptide exporter HAF-1 signals a mitochondrial UPR by activating the transcription factor ZC376.7 in C. elegans. *Mol Cell* **37**, 529-40.

Hensen, F., Cansiz, S., Gerhold, J. M. and Spelbrink, J. N. (2014). To be or not to be a nucleoid protein: a comparison of mass-spectrometry based approaches in the identification of potential mtDNA-nucleoid associated proteins. *Biochimie* **100**, 219-26.

Islam, M. S., Leissing, T. M., Chowdhury, R., Hopkinson, R. J. and Schofield, C. J. (2018). 2-Oxoglutarate-Dependent Oxygenases. *Annu Rev Biochem*.

Kawarada, L., Suzuki, T., Ohira, T., Hirata, S., Miyauchi, K. and Suzuki, T. (2017). ALKBH1 is an RNA dioxygenase responsible for cytoplasmic and mitochondrial tRNA modifications. *Nucleic Acids Res*.

Kollarova, J., Kostrouchova, M., Benda, A. and Kostrouchova, M. (2018). ALKB-8, a 2-Oxoglutarate-Dependent Dioxygenase and S-Adenosine Methionine-Dependent Methyltransferase Modulates Metabolic Events Linked to Lysosome-Related Organelles and Aging in C. elegans. *Folia Biol (Praha)* **64**, 46-58.

Kooistra, S. M. and Helin, K. (2012). Molecular mechanisms and potential functions of histone demethylases. *Nat Rev Mol Cell Biol* **13**, 297-311.

Kukat, C., Wurm, C. A., Spahr, H., Falkenberg, M., Larsson, N. G. and Jakobs, S. (2011). Super-resolution microscopy reveals that mammalian mitochondrial nucleoids have a uniform size and frequently contain a single copy of mtDNA. *Proc Natl Acad Sci U S A* **108**, 13534-9.

Liu, F., Clark, W., Luo, G., Wang, X., Fu, Y., Wei, J., Wang, X., Hao, Z., Dai, Q., Zheng, G. et al. (2016). ALKBH1-Mediated tRNA Demethylation Regulates Translation. *Cell* **167**, 1897.

Lu, Y., Rolland, S. G. and Conradt, B. (2011). A molecular switch that governs mitochondrial fusion and fission mediated by the BCL2-like protein CED-9 of Caenorhabditis elegans. *Proc Natl Acad Sci U S A* **108**, E813-22.

Melber, A. and Haynes, C. M. (2018). UPR(mt) regulation and output: a stress response mediated by mitochondrial-nuclear communication. *Cell Res* **28**, 281-295.

Meyer, K. D. and Jaffrey, S. R. (2014). The dynamic epitranscriptome: N6-methyladenosine and gene expression control. *Nat Rev Mol Cell Biol* **15**, 313-26.

Mossmann, D., Meisinger, C. and Vogtle, F. N. (2012). Processing of mitochondrial presequences. *Biochim Biophys Acta* **1819**, 1098-106.

Muller, T. A., Meek, K. and Hausinger, R. P. (2010). Human AlkB homologue 1 (ABH1) exhibits DNA lyase activity at abasic sites. *DNA Repair (Amst)* **9**, 58-65.

Muller, T. A., Struble, S. L., Meek, K. and Hausinger, R. P. (2018). Characterization of human AlkB homolog 1 produced in mammalian cells and demonstration of mitochondrial dysfunction in ALKBH1-deficient cells. *Biochem Biophys Res Commun* **495**, 98-103.

Nargund, A. M., Pellegrino, M. W., Fiorese, C. J., Baker, B. M. and Haynes, C. M. (2012). Mitochondrial import efficiency of ATFS-1 regulates mitochondrial UPR activation. *Science* **337**, 587-90.

Neupert, W. (2015). A perspective on transport of proteins into mitochondria: a myriad of open questions. *J Mol Biol* **427**, 1135-58.

Ougland, R., Jonson, I., Moen, M. N., Nesse, G., Asker, G., Klungland, A. and Larsen, E. (2016). Role of ALKBH1 in the Core Transcriptional Network of Embryonic Stem Cells. *Cell Physiol Biochem* **38**, 173-84.

Ougland, R., Lando, D., Jonson, I., Dahl, J. A., Moen, M. N., Nordstrand, L. M., Rognes, T., Lee, J. T., Klungland, A., Kouzarides, T. et al. (2012). ALKBH1 is a histone H2A dioxygenase involved in neural differentiation. *Stem Cells* **30**, 2672-82.

Pearce, S. F., Rebelo-Guiomar, P., D'Souza, A. R., Powell, C. A., Van Haute, L. and Minczuk, M. (2017). Regulation of Mammalian Mitochondrial Gene Expression: Recent Advances. *Trends Biochem Sci* **42**, 625-639.

Rajala, N., Gerhold, J. M., Martinsson, P., Klymov, A. and Spelbrink, J. N. (2014). Replication factors transiently associate with mtDNA at the mitochondrial inner membrane to facilitate replication. *Nucleic Acids Res* **42**, 952-67.

Reid, M. A., Dai, Z. and Locasale, J. W. (2017). The impact of cellular metabolism on chromatin dynamics and epigenetics. *Nat Cell Biol* **19**, 1298-1306.

Robert, X. and Gouet, P. (2014). Deciphering key features in protein structures with the new ENDscript server. *Nucleic Acids Res* **42**, W320-4.

Schermelleh, L., Carlton, P. M., Haase, S., Shao, L., Winoto, L., Kner, P., Burke, B., Cardoso, M. C., Agard, D. A., Gustafsson, M. G. et al. (2008). Subdiffraction multicolor imaging of the nuclear periphery with 3D structured illumination microscopy. *Science* **320**, 1332-6.

Schindelin, J., Arganda-Carreras, I., Frise, E., Kaynig, V., Longair, M., Pietzsch, T., Preibisch, S., Rueden, C., Saalfeld, S., Schmid, B. et al. (2012). Fiji: an open-source platform for biological-image analysis. *Nat Methods* **9**, 676-82.

Schmitt, S., Saathoff, F., Meissner, L., Schropp, E. M., Lichtmannegger, J., Schulz, S., Eberhagen, C., Borchard, S., Aichler, M., Adamski, J. et al. (2013). A semi-automated method for isolating functionally intact mitochondria from cultured cells and tissue biopsies. *Anal Biochem* **443**, 66-74.

Schneider, C. A., Rasband, W. S. and Eliceiri, K. W. (2012). NIH Image to ImageJ: 25 years of image analysis. *Nat Methods* **9**, 671-5.

Schofield, C. J. and Ratcliffe, P. J. (2004). Oxygen sensing by HIF hydroxylases. *Nat Rev Mol Cell Biol* **5**, 343-54.

Shpilka, T. and Haynes, C. M. (2018). The mitochondrial UPR: mechanisms, physiological functions and implications in ageing. *Nat Rev Mol Cell Biol* **19**, 109-120.

Sievers, F., Wilm, A., Dineen, D., Gibson, T. J., Karplus, K., Li, W., Lopez, R., McWilliam, H., Remmert, M., Soding, J. et al. (2011). Fast, scalable generation of high-quality protein multiple sequence alignments using Clustal Omega. *Mol Syst Biol* **7**, 539.

Songe-Moller, L., van den Born, E., Leihne, V., Vagbo, C. B., Kristoffersen, T., Krokan, H. E., Kirpekar, F., Falnes, P. O. and Klungland, A. (2010). Mammalian ALKBH8 possesses tRNA methyltransferase activity required for the biogenesis of multiple wobble uridine modifications implicated in translational decoding. *Mol Cell Biol* **30**, 1814-27.

van den Born, E., Vagbo, C. B., Songe-Moller, L., Leihne, V., Lien, G. F., Leszczynska, G., Malkiewicz, A., Krokan, H. E., Kirpekar, F., Klungland, A. et al. (2011). ALKBH8-mediated formation of a novel diastereomeric pair of wobble nucleosides in mammalian tRNA. *Nat Commun* **2**, 172.

Wang, P., Wu, J., Ma, S., Zhang, L., Yao, J., Hoadley, K. A., Wilkerson, M. D., Perou, C. M., Guan, K. L., Ye, D. et al. (2015). Oncometabolite D-2-Hydroxyglutarate Inhibits ALKBH DNA Repair Enzymes and Sensitizes IDH Mutant Cells to Alkylating Agents. *Cell Rep* **13**, 2353-2361.

Westbye, M. P., Feyzi, E., Aas, P. A., Vagbo, C. B., Talstad, V. A., Kavli, B., Hagen, L., Sundheim, O., Akbari, M., Liabakk, N. B. et al. (2008). Human AlkB homolog 1 is a mitochondrial protein that demethylates 3-methylcytosine in DNA and RNA. *J Biol Chem* **283**, 25046-56.

Wiznerowicz, M. and Trono, D. (2003). Conditional suppression of cellular genes: lentivirus vector-mediated drug-inducible RNA interference. *J Virol* **77**, 8957-61.

Wu, T. P., Wang, T., Seetin, M. G., Lai, Y., Zhu, S., Lin, K., Liu, Y., Byrum, S. D., Mackintosh, S. G., Zhong, M. et al. (2016). DNA methylation on N(6)-adenine in mammalian embryonic stem cells. *Nature* **532**, 329-33.

Yin, X. and Xu, Y. (2016). Structure and Function of TET Enzymes. *Adv Exp Med Biol* **945**, 275-302.

Yoneda, T., Benedetti, C., Urano, F., Clark, S. G., Harding, H. P. and Ron, D. (2004). Compartment-specific perturbation of protein handling activates genes encoding mitochondrial chaperones. *J Cell Sci* **117**, 4055-66.

Zhao, Q., Wang, J., Levichkin, I. V., Stasinopoulos, S., Ryan, M. T. and Hoogenraad, N. J. (2002). A mitochondrial specific stress response in mammalian cells. *EMBO J* **21**, 4411-9.

Zhuang, Q., Feng, T. and Coleman, M. L. (2015). Modifying the maker: Oxygenases target ribosome biology. *Translation (Austin)* **3**, e1009331.

Figures

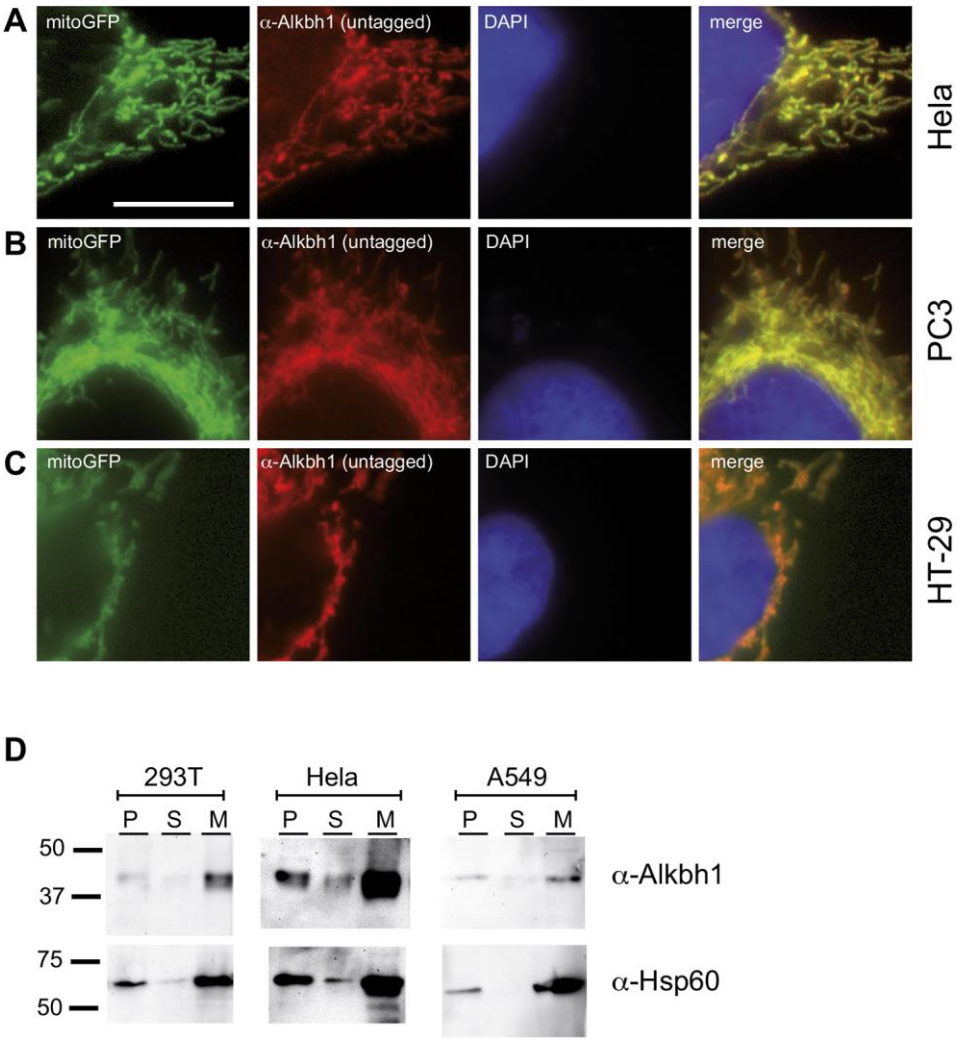

Figure 1

Immunofluorescence of overexpressed untagged human Alkbh1 with an anti-Alkbh1 antibody revealed extensive colocalisation with a mitochondrial GFP signal in Hela cells (**A**), PC3 cells (**B**) and HT-29 cells (**C**). Mitochondria were isolated using a pump-controlled cell rupture system (PCC) (Schmitt et al., 2013) from 293T cells, Hela cells and A549 cells. The cell debris (P), the crude cytosolic fraction (S) and crude mitochondria (M) of each cell line were loaded on a SDS-Page and subsequently immunoblotted for endogenous Alkbh1 and the mitochondrial marker protein Hsp60 (**D**). DNA-stain: DAPI. Scale bar = 10 μm.

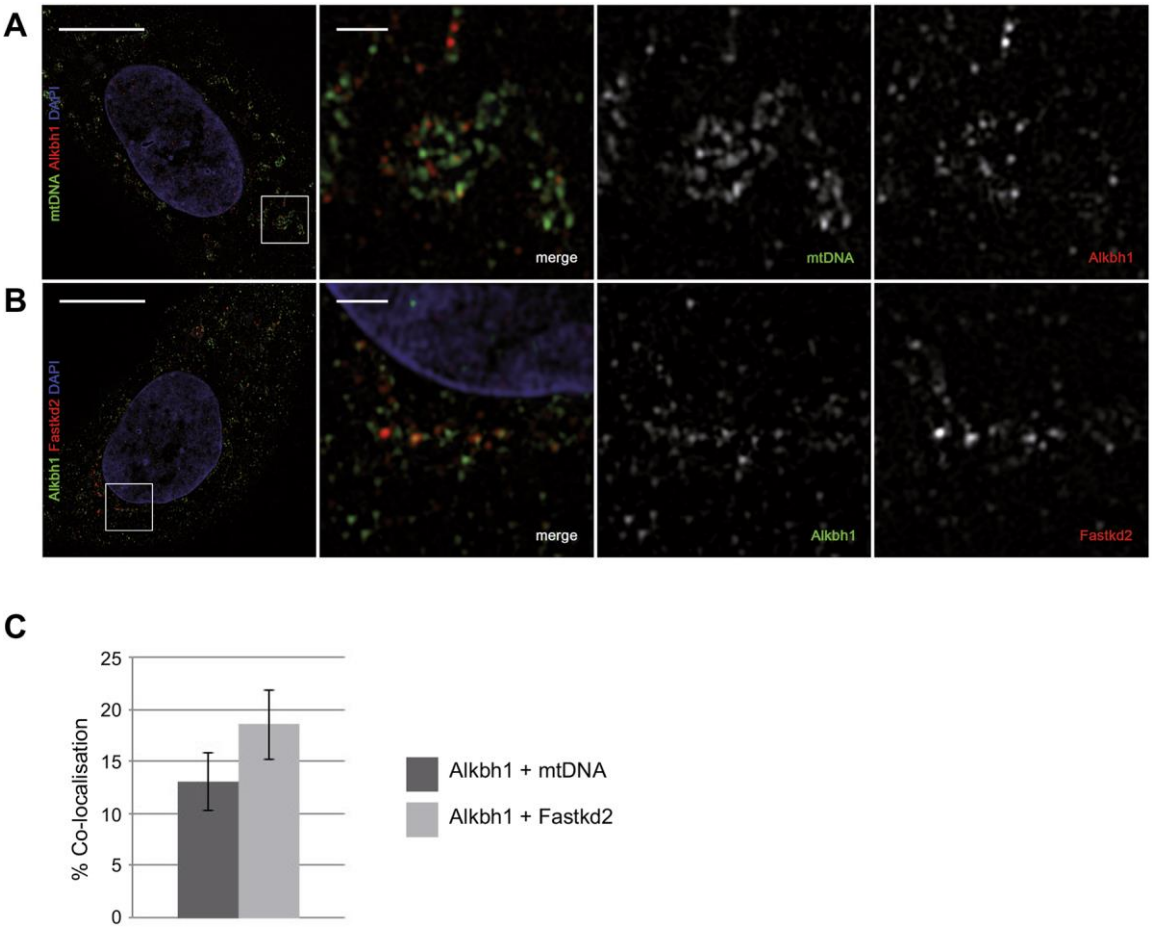

Figure 2

Analysis of endogenous Alkbh1 in A549 cells using super-resolution 3D-SIM imaging. Cells are immunostained with antibodies against Alkbh1 (red) and mtDNA (green) (**A**) or against Alkbh1 (green) and Fastkd2 (red) (**B**). DNA is counterstained with DAPI (blue). Central mid-sections of A549 cells are shown. Enlargements correspond to white boxes in whole-cell image. Scale bar (whole-cell): 10μm, scale bar (enlargement): 1μm. Six random whole cell images for each staining were analyzed for colocalisation as described in Materials and Methods. Percentage of Alkbh1 structures, which co-localize with mtDNA or Fastkd2 respectively, is given in the graph (**C**), showing a significantly higher colocalisation of Alkbh1 with Fastkd2 (unpaired *t*-test, *P* value: 0,009).

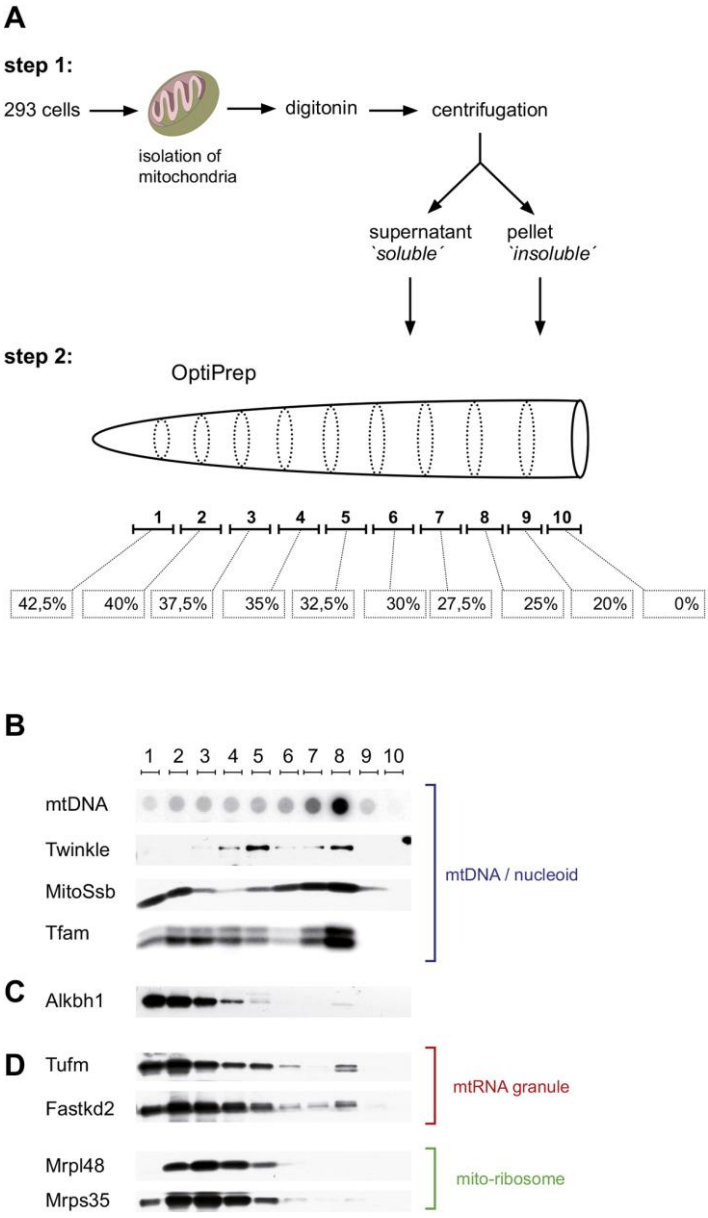

Figure 3

Density flotation gradient of purified and lysed 293 mitochondria. In step 1 mitochondria were isolated from 293 cells, lysed with digitonin and separated into supernatant and pellet fractions. In step 2, the pellet fraction was layered under an iodixanol (OptiPrep) step-gradient ranging from 42,5% to 0% iodixanol (**A**). After centrifugation the fractions 1-10 were collected and loaded on a SDS-Page and subsequently immunoblotted with antibodies as indicated in **B**, **C** and **D**. As previously described mtDNA, the helicase Twinkle, Tfam and mtSSB are co-localizing in one fraction (fraction 8) harboring actively replicating nucleoids (Gerhold et al., 2015; Rajala et al., 2014) (**B**). The majority of the observed Alkbh1 signal spreads over fractions 1-3 with weaker signals in 4 and residual signals in fraction 5 and 8 (**C**). The mtRNA granule markers Tufm and Fastkd2 show similar co-migration patterns in the gradient as Alkbh1 albeit their signals spread up to fractions 6 and 7, respectively, and show weak but clear signals in the nucleoid fraction 8 (**D**). Mito-ribosomal proteins Mrpl48 and Mrps35 are mainly detected in fraction 2-4, thus overlapping with Alkbh1, Fastkd2 and Tufm (**D**).

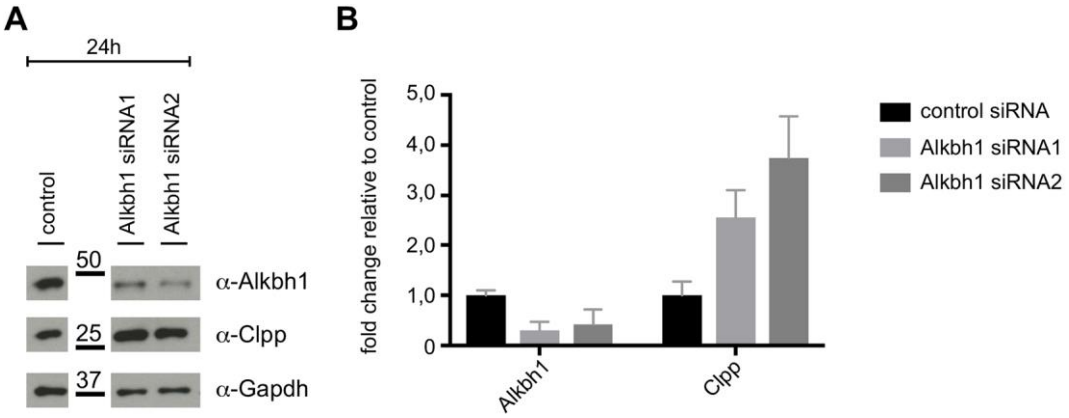

Figure 4

293 cells were transiently transfected with two different Alkbh1-specific siRNAs (Alkbh1 siRNA1, Alkbh1 siRNA2) and an unspecific control siRNA (control). 24 hours post-transfection cell lysates were analyzed in immunoblots with anti-Alkbh1 antibody, anti-Clpp antibody and anti-Gapdh antibody. Representative blots are shown in (**A**). The corresponding uncut blot is shown in **Fig. S4**. Relative expression levels of Alkbh1 and Clpp were quantified in western blots from three independent experiments using ImageJ (Schneider et al., 2012). Mean values relative to control siRNA are depicted in (**B**). Error bars indicate standard deviation.

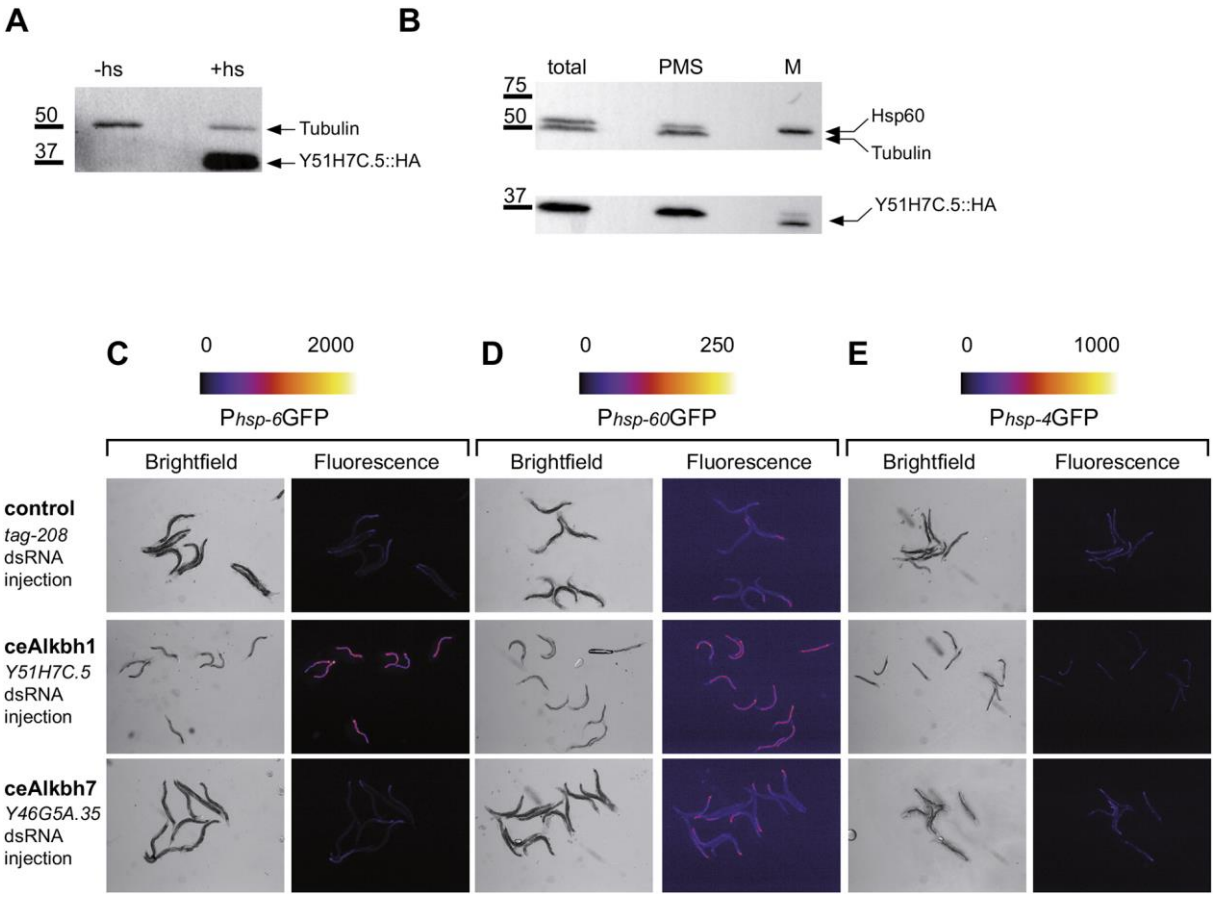

Figure 5

The transgenic line carrying the PHS:Y51H7C.5::HA transgene (ceAlkbh1) was heat-shocked and analyzed by western-blot using anti-Tubulin and anti-HA antibodies. (+HS: heat-shock; –HS: no heat-shock) (**A**). The transgenic line carrying the PHS:Y51H7C.5::HA transgene (ceAlkbh1) was heat-shocked and subjected to cell fractionation. 10% of the total lysate (total), 10% of the post mitochondrial supernatant (PMS) and 10% of the mitochondrial enriched fraction (M) were analyzed by SDS-PAGE and western-blot using anti-HSP-60 antibody (mitochondrial matrix marker), anti-Tubulin antibody (cytoplasmic marker) and using anti-HA antibodies to detect the Y51H7C.5::HA fusion protein (**B**).

C. elegans transgenic animals carrying the *Phsp-6GFP* (**C**), the *Phsp-60GFP* (**D**) or the *Phsp-4GFP* (**E**) transcriptional reporters were injected with dsRNA targeting *tag-208*, *Y51H7C.5* (ceAlkbh1) or *Y46G5A.35* (ceAlkbh7). 24 hours after injection, a lay off was performed and the progeny was analyzed by brightfield and fluorescent microscopy 96 hours later. Fluorescent images are shown in false color and the color scale is indicated above.

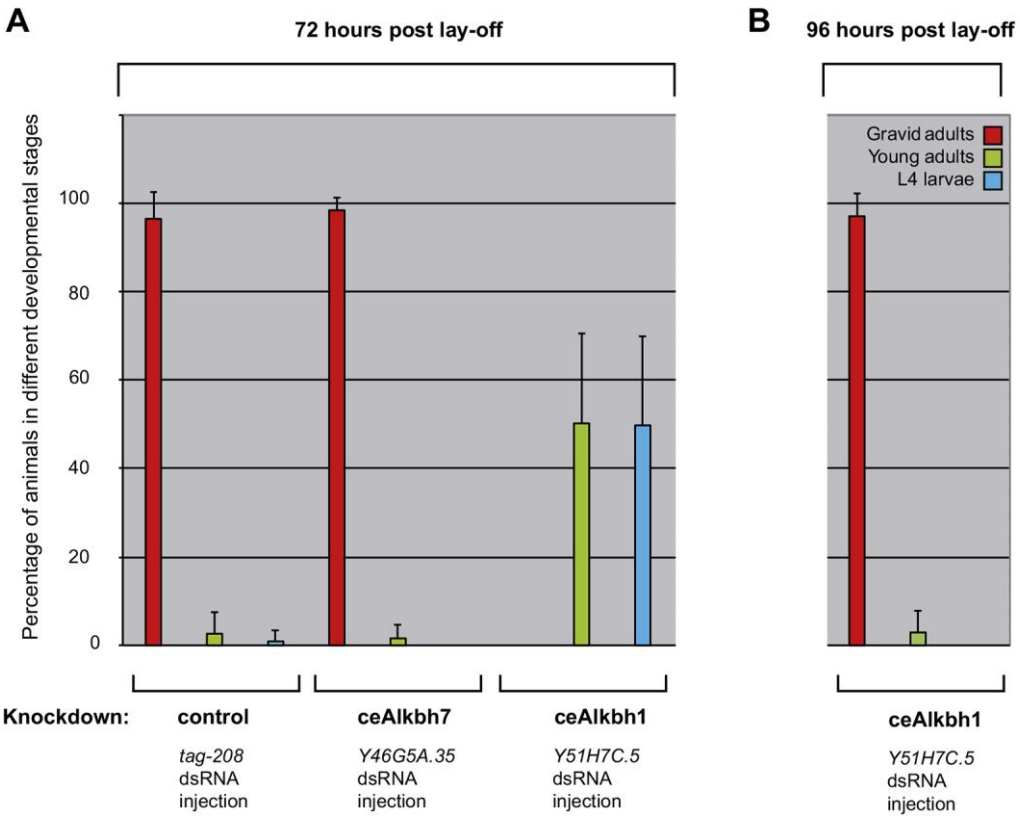

Figure 6

The developmental stages of the progeny of *tag-208*, *Y51H7C.5* (ceAlkbh1) or *Y46G5A.35* (ceAlkbh7) dsRNA injected animals were analyzed 72 hours (**A**) or 96 hours (**B**) post lay-off. The number of gravid adults, young adults and L4 larvae was quantified. Three independent experiments were performed with 2-3 plates analyzed in each experiment.

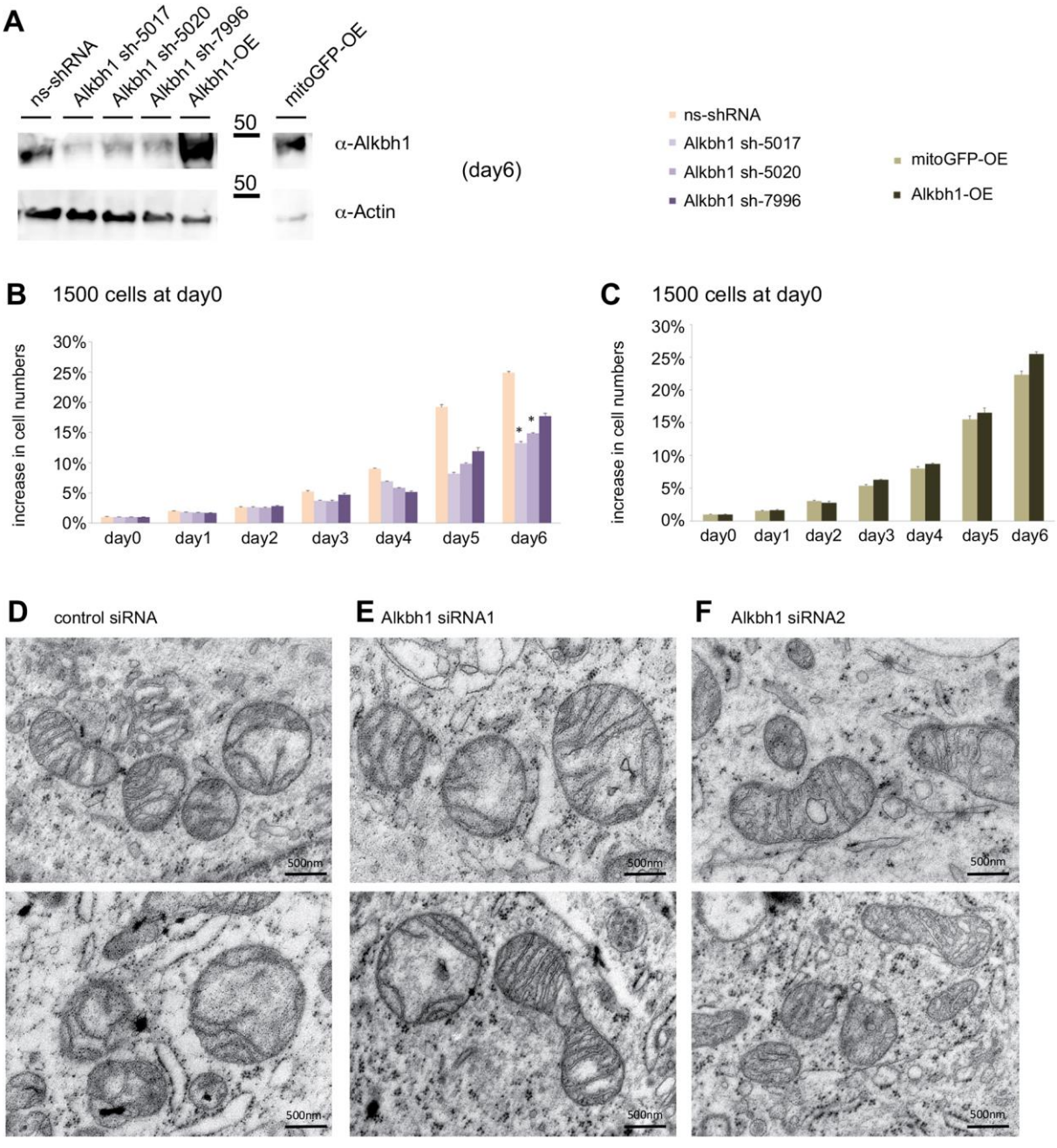

Figure 7

Stable doxycycline-inducible cell lines expressing either a non-silencing shRNA (ns-RNA), a specific Alkbh1 shRNA (Alkbh1 sh-5017, Alkbh1 sh-5020, Alkbh1 sh-7996), an untagged full-length Alkbh1 (Alkbh1-OE) or a mitochondrial GFP (mitoGFP) were collected six days post-induction. Individual cell lysates were loaded onto a SDS-Page and subsequently blotted. Western blots were stained with an anti-Alkbh1 antibody or with an anti-Actin antibody (**A**). Cell numbers of the inducible cell lines were monitored with an automated *Operetta* High-Content microscope in 24h intervals for six days post-induction starting with 1500 cells at day 0 (**B-C**).

293 cells transiently transfected with siRNAs (control siRNA, Alkbh1 siRNA1, Alkbh1 siRNA2) were subjected to EM analysis (**D-F**) and high-resolution respirometry to measure mitochondrial respiration (**G**). Oxygen consumption rates for each respiratory state (LEAK, OXPHOS, ETS) are depicted as mean values ± standard deviation of up to five independent experiments (**G**). Data were analyzed using unpaired t-test. Significance is shown as * $P < 0.05$, ** $P < 0.01$ and *** $P < 0.001$ compared to control siRNA.

Supplementary Figures

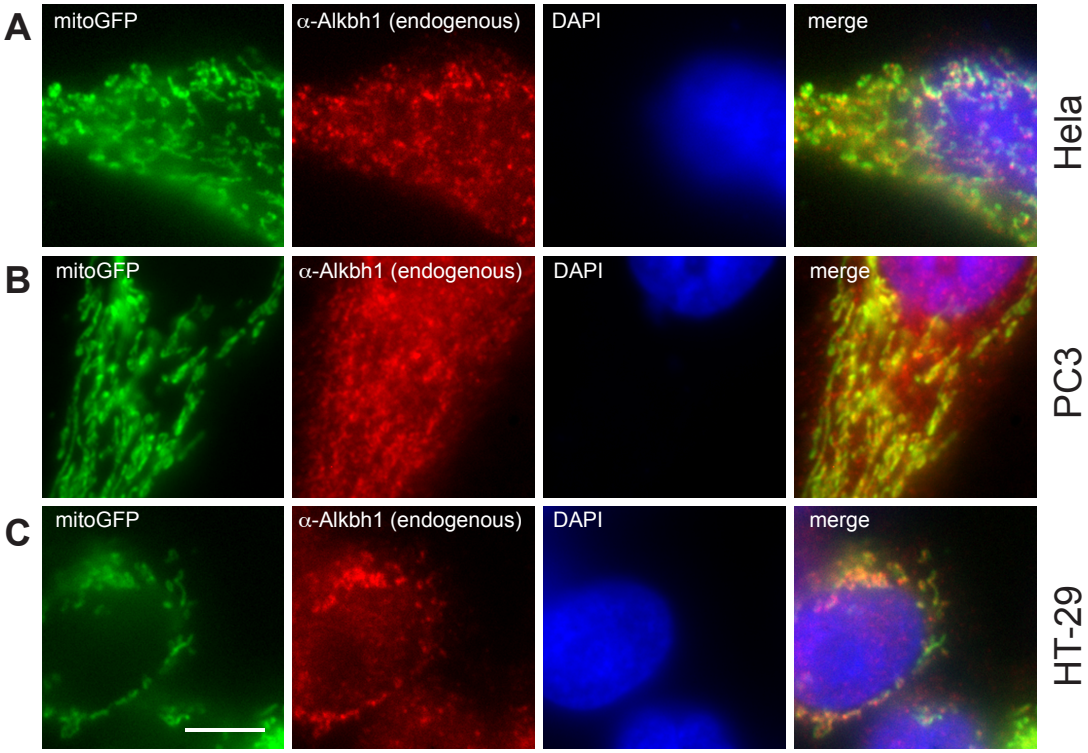

Figure S1

Immunofluorescence of endogenous human Alkbh1 with an anti-Alkbh1 antibody revealed colocalisation with a mitochondrial GFP signal in Hela cells (**A**), PC3 cells (**B**) and HT-29 cells (**C**). DNA-stain: DAPI. Scale bar = 10 μm.

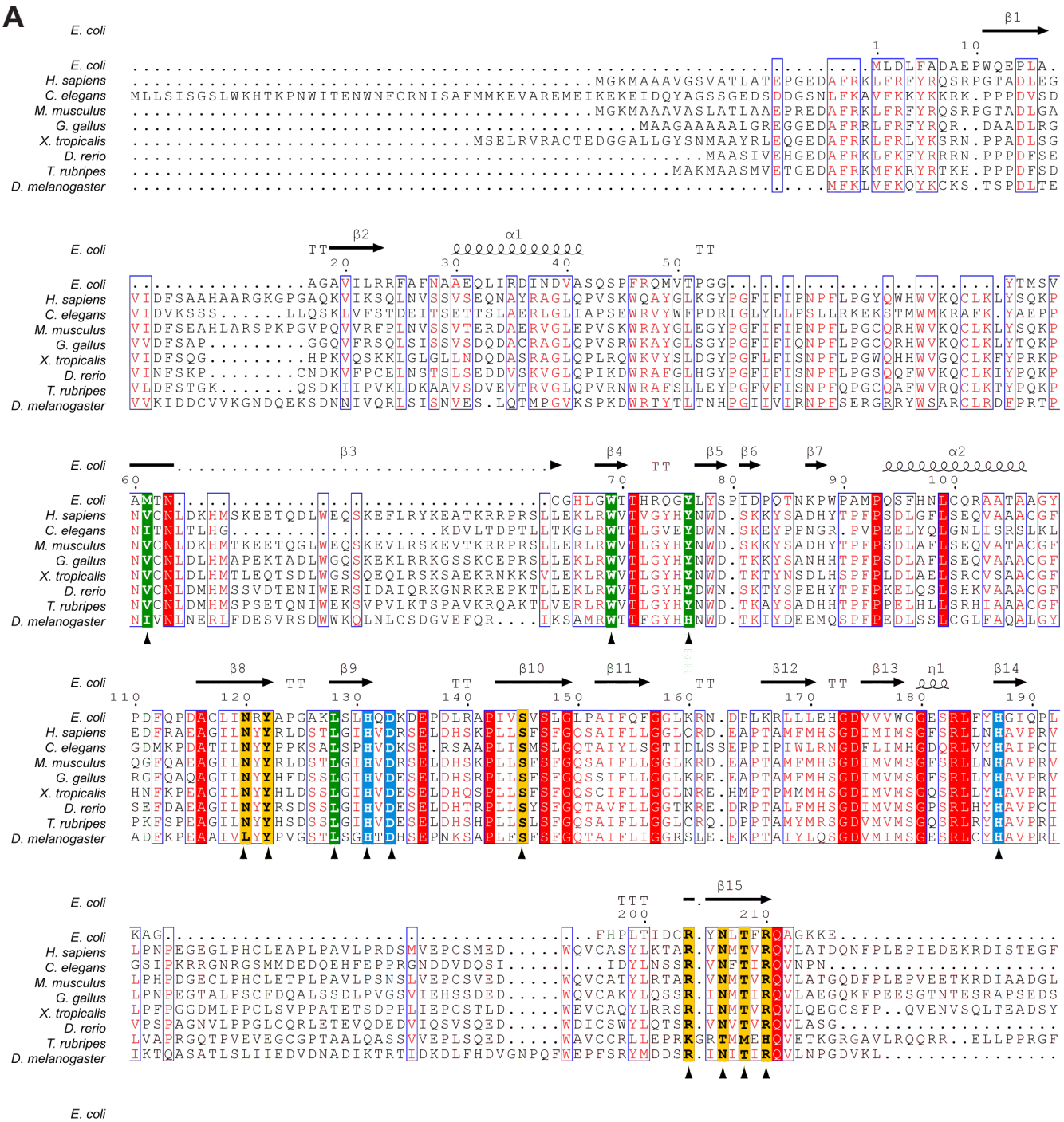

B

Organism	Uniprot No.	Sequence identity/similarity to *H. sapiens* Alkbh1 (in %)
H. sapiens	Q13686	-
C. elegans	E0DBL0	28.1 / 37.5
M. musculus (mouse)	P0CB42	82.8 /90.7
G. gallus (chicken)	Q5F3E4	66.0 / 76.6
X. tropicalis (xenopus)	F6WM70	53.3 / 65.2
D. rerio (zebrafish)	E9QHS2	51.4 / 65.8
T. rubripes (pufferfish)	A0A3B5KTL3	49.7 / 63.9
D. melanogaster (fruit fly)	Q7KUZ2	30.6 / 45.7
E. coli	P05050	13.5 / 22.7

Figure S2

Sequence conservation of Alkbh1 homologs. Sequence alignment generated with Clustal Omega (Sievers et al., 2011) and annotated manually and using Espript (Robert and Gouet, 2014) (**A**). The numbering and secondary structure assignment on top of the alignment corresponds to the structure of the full-length E. coli Alkb residues 1-216 (PDB code 3KHC; Uniprot: P05050). Conserved His and Asp residues coordinating the Fe^{2+} are highlighted in blue, residues involved in interactions with 2OG and lining the active site are highlighted in yellow and green, respectively. These residues are also marked with an arrow. Other fully conserved and similar residues are shaded and colored red, respectively. Please note the hAlkbh1 and ceAlkbh1 homologues are about 200 residues larger in size compared to EcAlkB, which corresponds most likely to additional secondary structure elements and/or subdomains to the conserved "jelly-role" folding architecture. Sequence identities and similarities between Alkbh1 homologues calculated using EMBOSS (**B**).

```
H. sapiens  --MAGTGLLAL-RTLPGPSWVRGSGPSVLSRLQDAAVVRPGFLSTAEEETLSRELEPELR
C. elegans  MKITPRTLQHLIKFHNLELWPKD----LAETMKTCCYVKKDFITEAEEKSLLVDVEPHMK
              ::   *  * :      * :.    : . :: .. *: .*:: ***::*  ::**.::

H. sapiens  RRRYEYDHWDAAIHGFRETEKSRWSEASRAILQRVQAAAFGPGQTLLSSVHVLDLEARGY
C. elegans  RLRYEKSHWDDAIHLYREREQRKWRDENLEVISRIRSESFGANTEHLTYVHILDLHKDGV
            * *** .*** *** :** *: :* : .  ::.*::: :** .   *: **:***.  *
               H D
H. sapiens  IKPHVDSIKFCGATIAGLSLLSPSVMRLVHTQEPGEW-LELLLEPGSLYILRGSARYDFS
C. elegans  IKPHIDAIRYCGDVITGVSLLSDAIMRLRHKDQKDELIMDLLMPRRSLYRLGGPGRYDFT
            ****:*:*::** .*:*:**** ::*** *.:: .*  ::**:   *** * * .****:
               H
H. sapiens  HEILRDEESFFGERRIPRGRRISVICRSLPEGMGPGESGQP-----PPAC-
C. elegans  HEVLGEQESVWNGEQVPRERRISIICRDLPKVANRQTAEEEIKLKPIPEEI
            **:* ::**.:. .::** ****:***.**:  .   : :       *
```

Figure S3

Clustal Omega alignments (Sievers et al., 2011) of the *C. elegans* Alkbh7 sequence with the human ortholog revealed 36,1% identical amino acids.

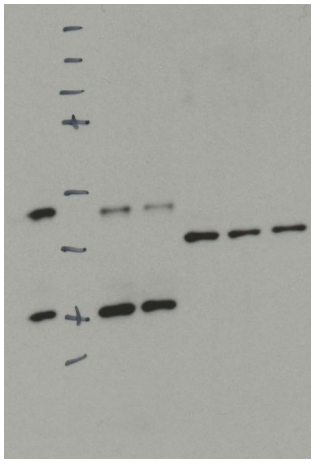

Figure S4

Corresponding uncut western blot, which is shown in parts in Figure 4.

Supplementary Figures

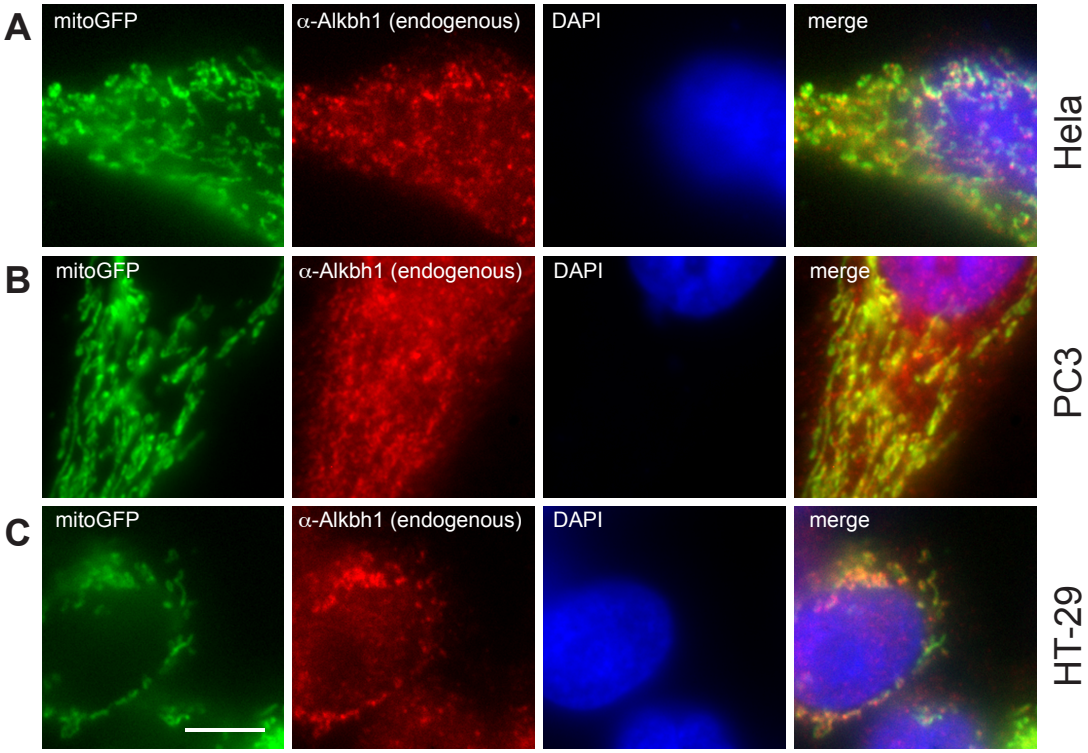

Figure S1

Immunofluorescence of endogenous human Alkbh1 with an anti-Alkbh1 antibody revealed colocalisation with a mitochondrial GFP signal in Hela cells (**A**), PC3 cells (**B**) and HT-29 cells (**C**). DNA-stain: DAPI. Scale bar = 10 μm.

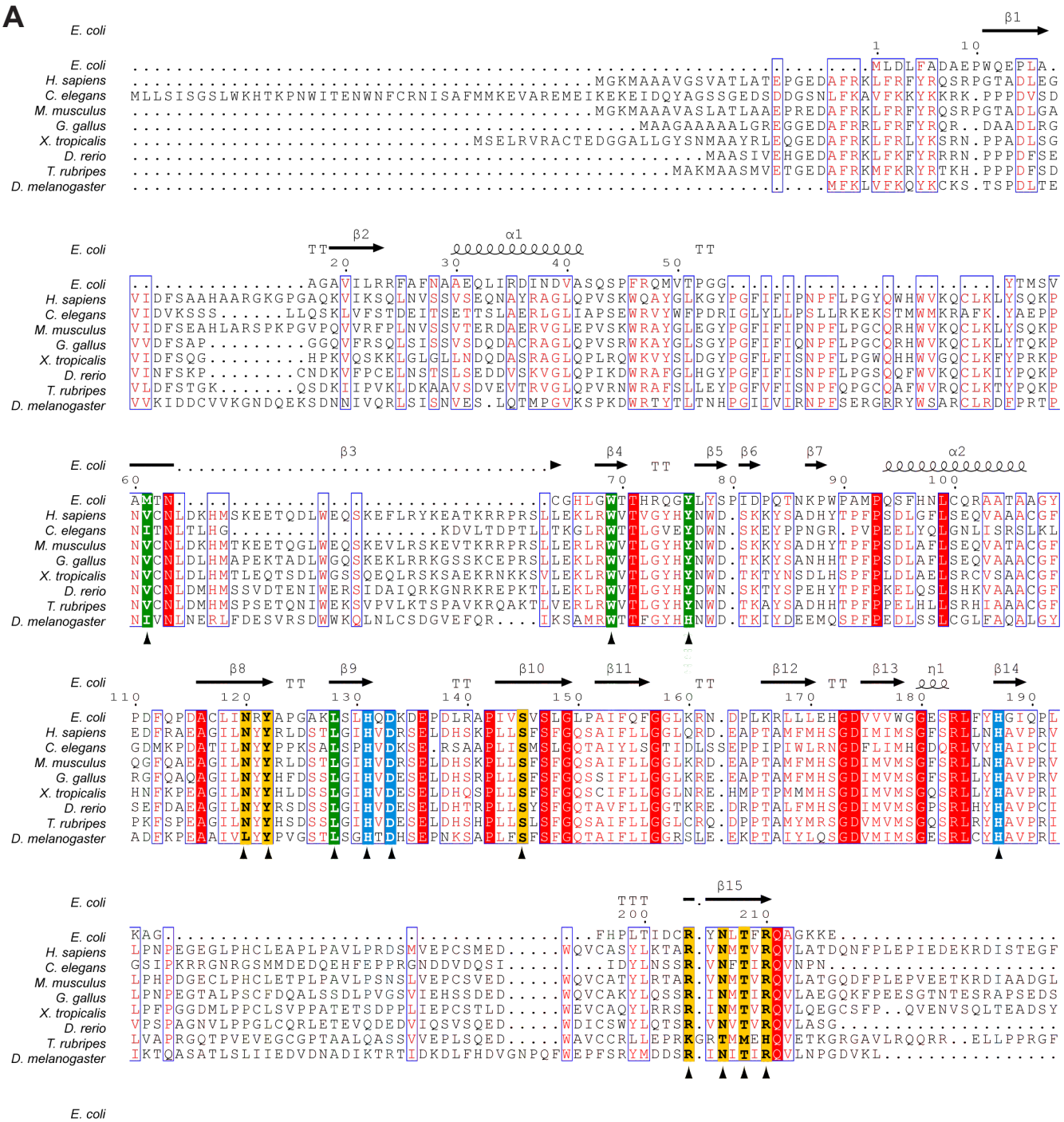

B

Organism	Uniprot No.	Sequence identity/similarity to *H. sapiens* Alkbh1 (in %)
H. sapiens	Q13686	-
C. elegans	E0DBL0	28.1 / 37.5
M. musculus (mouse)	P0CB42	82.8 /90.7
G. gallus (chicken)	Q5F3E4	66.0 / 76.6
X. tropicalis (xenopus)	F6WM70	53.3 / 65.2
D. rerio (zebrafish)	E9QHS2	51.4 / 65.8
T. rubripes (pufferfish)	A0A3B5KTL3	49.7 / 63.9
D. melanogaster (fruit fly)	Q7KUZ2	30.6 / 45.7
E. coli	P05050	13.5 / 22.7

Figure S2

Sequence conservation of Alkbh1 homologs. Sequence alignment generated with Clustal Omega (Sievers et al., 2011) and annotated manually and using Espript (Robert and Gouet, 2014) (**A**). The numbering and secondary structure assignment on top of the alignment corresponds to the structure of the full-length E. coli Alkb residues 1-216 (PDB code 3KHC; Uniprot: P05050). Conserved His and Asp residues coordinating the Fe^{2+} are highlighted in blue, residues involved in interactions with 2OG and lining the active site are highlighted in yellow and green, respectively. These residues are also marked with an arrow. Other fully conserved and similar residues are shaded and colored red, respectively. Please note the hAlkbh1 and ceAlkbh1 homologues are about 200 residues larger in size compared to EcAlkB, which corresponds most likely to additional secondary structure elements and/or subdomains to the conserved "jelly-role" folding architecture. Sequence identities and similarities between Alkbh1 homologues calculated using EMBOSS (**B**).

```
H. sapiens  --MAGTGLLAL-RTLPGPSWVRGSGPSVLSRLQDAAVVRPGFLSTAEEETLSRELEPELR
C. elegans  MKITPRTLQHLIKFHNLELWPKD----LAETMKTCCYVKKDFITEAEEKSLLVDVEPHMK
              ::   *  * :      * :.    : . :: .. *: .*:: ***::*  ::**.::

H. sapiens  RRRYEYDHWDAAIHGFRETEKSRWSEASRAILQRVQAAAFGPGQTLLSSVHVLDLEARGY
C. elegans  RLRYEKSHWDDAIHLYREREQRKWRDENLEVISRIRSESFGANTEHLTYVHILDLHKDGV
            * *** .*** *** :** *: :* : .  ::.*::: :** .   *: **:***.  *
               H D
H. sapiens  IKPHVDSIKFCGATIAGLSLLSPSVMRLVHTQEPGEW-LELLLEPGSLYILRGSARYDFS
C. elegans  IKPHIDAIRYCGDVITGVSLLSDAIMRLRHKDQKDELIMDLLMPRRSLYRLGGPGRYDFT
            ****:*:*::** .*:*:**** ::*** *.:: .*  ::**:   *** * * .****:
               H
H. sapiens  HEILRDEESFFGERRIPRGRRISVICRSLPEGMGPGESGQP-----PPAC-
C. elegans  HEVLGEQESVWNGEQVPRERRISIICRDLPKVANRQTAEEEIKLKPIPEEI
            **:* ::**.:. .::** ****:***.**:  .   : :       *
```

Figure S3

Clustal Omega alignments (Sievers et al., 2011) of the *C. elegans* Alkbh7 sequence with the human ortholog revealed 36,1% identical amino acids.

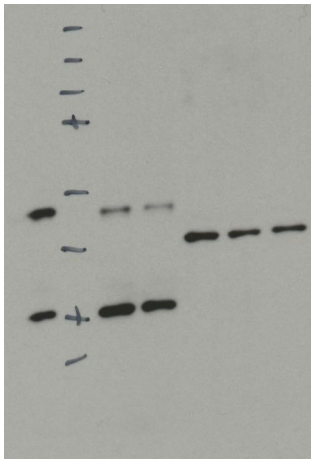

Figure S4

Corresponding uncut western blot, which is shown in parts in Figure 4.

Table S1

	Dilutions	
Antibody	Western blotting	Immunoflourescence
anti-Alkbh1 (ab49738, *Abcam*)	1:500	1:100
anti-Alkbh1 (ab126596, *Abcam*)	1:500	1:100
anti-DNA (AC-30-10, *Progen*)		1:15
anti-Fastkd2 (17464-1-AP, *Proteintech*)	1:1000	1:100
anti-GFP (11814460001, *Roche*)	1:500	
anti-Hsp60 (ab46798, *Abcam*)	1:500-1:1000	
anti-Tfam (ab119684, *Abcam*)	1:1000	
anti-Gapdh (2118 S, *Cell Signaling*)	1:5000	
anti-Actin (sc-1616, *Santa Cruz*)	1:500	
anti-Hsp60 (sc-1052, *Santa Cruz*)	1:2000	
anti-Clpp (ab124822, *Abcam*)	1:1000	
anti-Mrs35 (ab182160, *Abcam*)	1:1000	
anti-Mrpl48 (ab194826, *Abcam*)	1:1000	
anti-Ssbp1 (HPA002866, *Sigma*)	1:1000	
anti-Tufm (ab175199, *Abcam*)	1:1000	
Alexa Flour 488 anti-rat IgG (*Life Technologies*)		1:500
Alexa Flour 594 anti-rat IgG (*Life Technologies*)		1:500
Alexa Flour 594 anti-rabbit IgG (*Life Technologies*)		1:500
Alexa Flour 488 anti-mouse IgG (*Life Technologies*)		1:500
anti-HA (H9658, *Sigma-Aldrich*)	1:2000	
Anti-HSP60 *(Hadwiger et al., 2010)*	1:2000	
anti-Twinkle (Gerhold et al., 2015) (gift from Anu SuomalainenWartiovaara, University of Helsinki, Finland),	1:1000	
anti-Tubulin (T6199, *Sigma-Aldrich*)	1:10000	